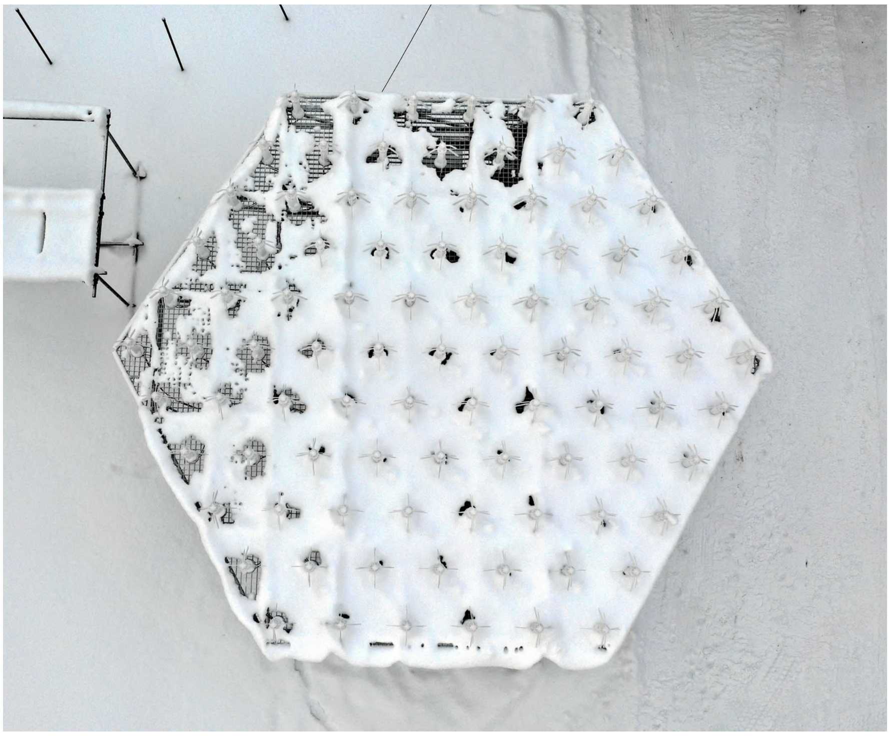

# EISCAT

## EUROPEAN INCOHERENT SCATTER
## SCIENTIFIC ASSOCIATION

## ANNUAL REPORT 2019 – 2020

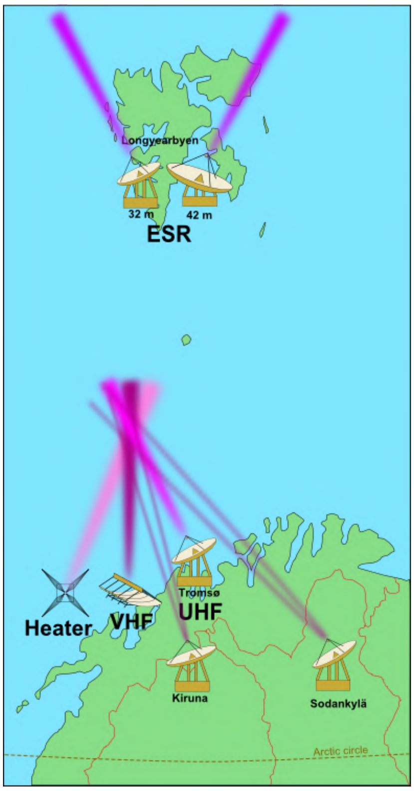

# EISCAT Radar Systems

| **Location** | **Tromsø** | | **Kiruna** | **Sodankylä** | **Longyearbyen** | |
|---|---|---|---|---|---|---|
| **Geographic coordinates** | 69°35′N<br>19°14′E | | 67°52′N<br>20°26′E | 67°22′N<br>26°38′E | 78°9′N<br>16°1′E | |
| **Geomagnetic inclination** | 77°30′N | | 76°48′N | 76°43′N | 82°6′N | |
| **Invariant latitude** | 66°12′N | | 64°27′N | 63°34′N | 75°18′N | |
| **Band** | UHF | VHF | VHF | VHF | UHF | |
| **Frequency (MHz)** | 929 | 224 | 224 | 224 | 500 | |
| **Maximum bandwidth (MHz)** | 8 | 3 | 8 | 8 | 10 | |
| **Transmitter** | 2 klystrons | 1 klystron | - | - | 16 klystrons | |
| **Channels** | 6 | 6 | 6 | 6 | 12 | |
| **Peak Power (MW)** | 2.0 | 1.6 | - | - | 1.0 | |
| **Average power (MW)** | 0.25 | 0.20 | - | - | 0.25 | |
| **Pulse duration (ms)** | 0.001–2.0 | 0.001–2.0 | - | - | 0.0005–2.0 | |
| **Phase coding** | binary | binary | binary | binary | binary | |
| **Minimum interpulse (ms)** | 1.0 | 1.0 | - | - | 0.1 | |
| **Digital processing** | 14 bit ADC on IF, 32 bit complex autocorrelation functions, parallel channels | | | | | |
| | | | | | **Antenna 1** | **Antenna 2** |
| **Antenna** | parabolic dish<br>32 m steerable | parabolic cylinder<br>120 m × 40 m steerable | parabolic dish<br>32 m steerable | parabolic dish<br>32 m steerable | parabolic dish<br>32 m steerable | parabolic dish<br>42 m fixed |
| **Feed system** | Cassegrain | line feed<br>128 crossed dipoles | crossed dipole | crossed dipole | Cassegrain | Cassegrain |
| **System temperature (K)** | 90 | 250 | 100 | 100 | 80 | 65 |
| **Gain (dBi)** | 48.1 | 46 | 35.4 | 35.4 | 42.5 | 44.8 |
| **Polarisation** | circular | circular | any | any | circular | circular |

# EISCAT Heating Facility (Tromsø)

Frequency range: 4.0 MHz to 8.0 MHz, Maximum transmitter power: 12×0.1 MW, Antennas: Array 1 (5.5 MHz to 8.0 MHz) 30 dBi, Array 2 (4.0 MHz to 5.5 MHz) 24 dBi, Array 3 (5.5 MHz to 8.0 MHz) 24 dBi. Additionally, a Dynasonde is operated at the heating facility.

---

**Cover picture:** EISCAT_3D PET AU in Kiruna (Photo: Craig Heinselman).

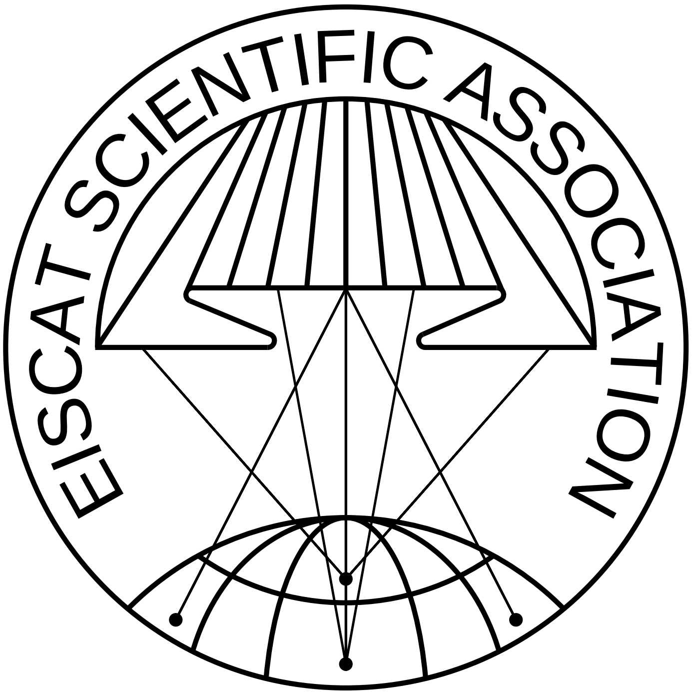

# EISCAT Scientific Association
# 2019–2020

*The EISCAT Scientific Association exists to provide scientists with access to incoherent scatter radar facilities of the highest technical standard*

- *by developing and operating a continuing program of observatory measurements in cooperation with other ground-based and space-borne instruments and as part of the global network of incoherent scatter radars, the EISCAT Scientific Association seeks to provide a long-term database of ionospheric measurements of the highest quality.*
- *by supporting and operating the particular experiments of individual, and groups of, visiting scientists, EISCAT seeks to allow its users to address the widest possible range of research activities particularly in the areas of geospace and basic plasma physics.*
- *by providing leadership in the design and construction of hardware and software to support these goals, the EISCAT Scientific Association seeks to provide educational opportunities for young scientists and to foster appropriate Knowledge Transfer and Economic Impact.*
- *by developing and maintaining a well-founded science strategy, EISCAT seeks to provide a framework for the development of EISCAT-supported science and for the evaluation and development of scientific programs within the overall field.*

*The scientific strategy of EISCAT is to understand the various forms of coupling between the Sun, the interplanetary medium, the terrestrial magnetosphere, ionosphere, and atmosphere of the high-latitude regions, natural and anthropogenic forcing, and related plasma physics and dynamics, and to achieve the necessary knowledge, understanding, principles, and techniques which would allow mankind to monitor, predict, and mitigate such processes within the next 30 years.*

*The specific goals of EISCAT are to develop large-scale facilities, techniques, and methods and, together with other ground-based and space-borne instruments, and as part of the global network of incoherent scatter and other middle and upper atmosphere radars, to encourage and undertake high quality research related to the global goal through studies addressing*

- *behaviour and energy budget of the high-latitude regions, including space weather effects.*
- *fundamental plasma physics and dynamic processes in the near-Earth space environment.*
- *trends in atmospheric and ionospheric conditions, including long-term global change.*
- *properties and dynamics of the interplanetary environment.*
- *parametrisation of these processes and the development of techniques for their prediction.*

*The investments and operational costs of EISCAT are shared between:*

*China Research Institute of Radiowave Propagation, People's Republic of China*
*National Institute of Polar Research, Japan*
*Norges forskningsråd, Norway*
*Suomen Akatemia, Finland*
*UK Research and Innovation, United Kingdom*
*Vetenskapsrådet, Sweden*

# Contents

# Director's pages

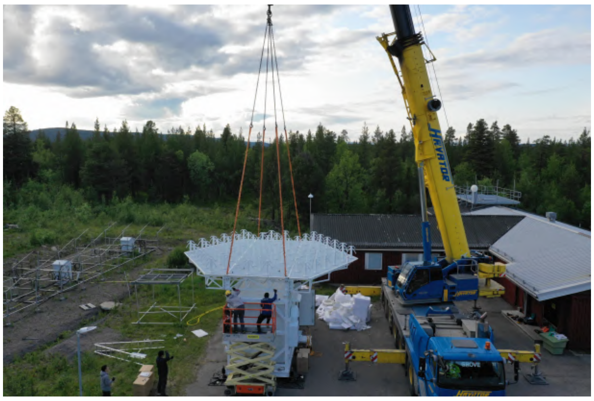

Figure 1: PET AU Installation in Kiruna.

EISCAT continues to provide its user community with incoherent scatter radar (ISR) systems and data of the highest technical quality at key locations in the Geospace environment. The presently operating systems, in Ramfjordmoen (Norway), Kiruna (Sweden), Sodankylä (Finland) and Longyearbyen (Svalbard) are, to varying degrees, showing their ages and have suffered from a number of mostly repairable failures. This has resulted in some short-term data gaps and performance limitations. For instance, several antenna issues have limited operations: the waveguide for the Ramfjordmoen VHF system had arcing problems, the pintle bearings in both the Ramfjordmoen UHF and the Sodankylä antennas have needed attention, and the UHF antenna had a catastrophic failure of one of its gear boxes. This gearbox failure led EISCAT to remove the identical unit from the Kiruna antenna to effect repairs, thus limiting the motion of that antenna during operations. Similarly, the antenna fields for the Heating facility have needed significant repairs to maintain operational status. Nonetheless, EISCAT has maintained successful measurement campaigns for Common Programmes, Special Programmes, and Peer-review Programmes throughout this period.

A great deal of progress has also been made toward the implementation of the EISCAT_3D systems. The Project Engineering and Test (PET) Antenna Unit (AU) was delivered and installed at the Kiruna site during the summer of 2019, following successful factory testing in January of that year. Subsequent testing and integration of other subsystems in the PET AU verified the performance of the antenna elements under realistic conditions, but also revealed areas for improvement in the design of aspects of the equipment container portion of the AU.

First article deliveries of the First Stage Receive Unit (FSRU), the Pulse and Steering Control Unit (PSCU) and the Transmit Unit (TU) were also made and tested in the PET AU. The hardware integration and testing efforts were also supported by the design of low-level software to ensure proper functioning of these systems. The speed of the overall project progress was impacted somewhat by the restrictions imposed in response to the COVID-19 pandemic, but the hardware and software development efforts were able to continue at a somewhat reduced pace.

In parallel with the radar hardware and software development, the EISCAT_3D site preparation work also proceeded. The ground preparation for both the Skibotn Transmit/Receive site and the Karesuvanto Receive-only site were completed and tested for settlement. The Kaiseniemi Receive-only site was delayed by difficulties in obtaining all the necessary permissions to build, though at the end of 2020 the final decisions appear to be imminent.

*Craig Heinselman*
*Director*
*EISCAT Scientific Association*

Figure 2: PET AU under winter conditions.

# Scientific highlights and list of publications 2019–2020

## Auroral studies

### Polarisation electric field inside auroral patches: simultaneous experiment of EISCAT radars and KAIRA

The primary focus of a study by Takahashi et al. (2019) was the motion of auroral patches and the polarisation electric field generated therein observed on 9 November 2015 in an experiment using the European incoherent scatter (EISCAT) radars (Figure 3), Kilpisjärvi Atmospheric Imaging Receiver Array (KAIRA), and an all-sky imager simultaneously. Based on the all-sky imager data, the drift speed of the auroral patches corresponded to a southward electric field of $(14.1 \pm 3.7)\,\mathrm{mV/m}$ to $(17.2 \pm 4.5)\,\mathrm{mV/m}$. The convective electric field derived from the EISCAT radars and KAIRA observation was approximately 14.6 mV/m in the southward direction. This suggests that the spatial distribution of the auroral patches reflects the distribution of the cold plasma in the magnetosphere. The electron density and the height-integrated Hall conductance at 80 km to 120 km were enhanced by a factor of 2 to 4 inside the auroral patches. In this situation, a polarisation electric field was generated therein. Enhanced ion velocities due to the polarisation electric field was observed at up to 200 km altitude; however, the absolute values of the ion velocities were approximately 40 % of what was expected from the polarisation electric field. A field-aligned current (FAC) from $5\,\mu\mathrm{A/m^2}$ to $10\,\mu\mathrm{A/m^2}$ in the edges of the auroral patches could explain the weakening of the polarisation electric field. Since a FAC of that order of magnitude corresponded with that observed by the Swarm satellite, it was suggested that the polarisation electric field was weakened by the FAC. Furthermore, the polarisation electric field propagated upward from the dynamo region to at least 200 km.

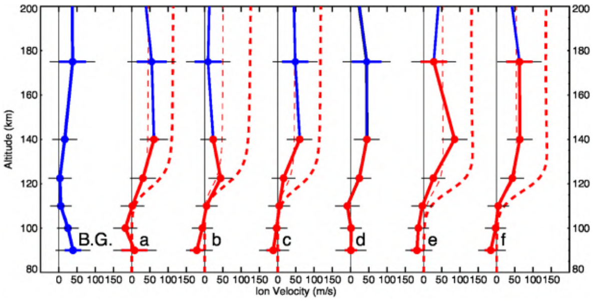

Figure 3: Height profile of $v_{\mathrm{iP}}$ for each auroral patch observed by the VHF radar. Red dots show the ion velocity influenced by the auroral patches. The leftmost line is defined as the background ion velocity averaged from 02:47:30 to 02:48:30 UT. The blue and red bars show the measurement error. The black bar shows the fluctuation related to the neutral wind. The red thick and thin dashed line is the estimated ion velocity for $E_{\mathrm{P}}$ and the 40 % weakened $E_{\mathrm{P}}$.

### Observations of precipitation energies during different types of pulsating aurora

Tesema et al. (2020) used electron density measurements from the EISCAT VHF and UHF radars, in combination with the Cosmic Noise Absorption (CNA) measurements by the Kilpisjärvi Atmospheric Imaging Receiver Array (KAIRA) and all-sky camera images to investigate three different types of pulsating aurora (PsA). The CNA measurements serve as a proxy for signatures of high (more than 10 keV) energetic particle precipitation in the D-region. Pulsating aurora is defined as a quasi-periodic low-intensity (a few kilorayleigh) diffuse emissions, which switches on and off with periods of a few seconds to a few tens of seconds. They have been categorized into three main types: amorphous pulsating aurora (APA), patchy pulsation aurora (PPA) and patchy aurora (PA) based on the spatial extent of the pulsations and structural

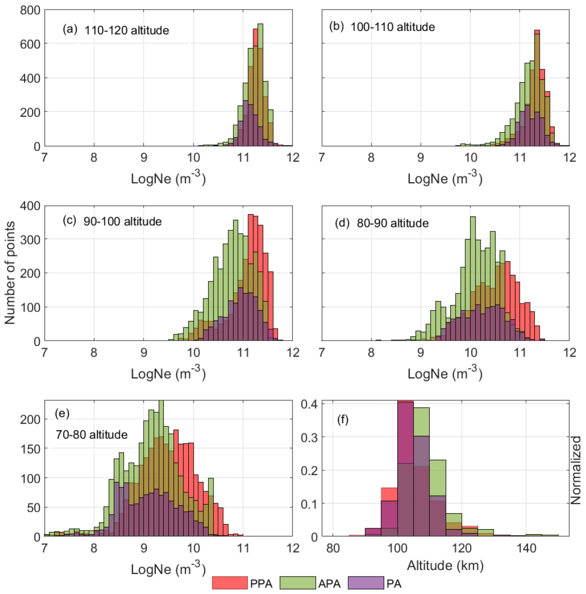

Figure 4: Histogram of EISCAT electron density measurements average between (a) 110 km and 120 km, (b) 100 km and 110 km, (c) 90 km and 100 km, (d) 80 km and 90 km, (e) 70 km and 80 km, and (f) altitude of maximum electron density during different types of pulsating aurora.

stability. The exact source and mechanism driving the different PsAs is still unclarified. Tesema et al. (2020) used a statistical study of 92 PsAs, occurring between 20 MLT and 10 MLT, to evaluate the energy spectra of the particle precipitation associated with each type. Figure 4 shows several histograms derived from EISCAT data showing the ionospheric electron density, averaged over 10 km wide bins for the three different types of PsAs. They found that on average, the precipitating energy spectra during the three types of PsAs have significant differences. In particular, they highlighted that most of the differences in ionisation levels occurred below 100 km altitude implying precipitation of relativistic electrons with a higher energy ( around 200 keV) for PPA and PA than for APA. The authors also speculate that, due to the high energies involved, PsAs (in particular PPAs) may contribute significantly to the destruction of ozone in the lower D-region.

## Expanding Auroral Loop

A new scenario is presented by Haerendel (2019) for the energy supply to the auroral acceleration process. It applies to auroral arcs, which are propagating into regions of magnetic fields with shears. This pertains in particular to expanding U-loops or other active protrusions. A Poynting flux, emerging out of the interior of the associated current system with strongly sheared field, flows into the auroral acceleration region or fracture zone. One half of the energy is consumed by the acceleration process. The other half flows (mainly upward) into the current sheet and is expended by shearing the newly incorporated field into the direction of the internal field. This is enabled by the magnetic connectivity being broken inside the region of parallel electric potential drops. The latter are formally attributed to the presence of an anomalous resistivity in the auroral current sheet. Simple relations describe the energy transport and consumption. An important quantity is the width of the arc. It follows from the balance of the energy transport inside and out of the acceleration region. Since the process involves first breaking of the field lines, to be followed by building up shear stresses, the name "constructive magnetic fractures" has been chosen for distinguishing it from "destructive fractures", which applies to embedded arcs. The model is inspired by plasma velocity components measured in the European Incoherent Scatter (EISCAT) common volume and simultaneous optical video of aurora. See Figure 5.

## Estimation of the emission altitude of pulsating aurora by using the five-wavelength photometer

Using a ground-based five-wavelength photometer, which has been operative in Tromsø, Norway since February 2017, Kawamura et al. (2020) have statistically analysed the lifetime of O($^1$S) to reveal the emission altitude of pulsating aurora (PsA). For the statistics, they extracted intervals of PsA using an EMCCD all-sky imager on 37 nights during three months from January to March, 2018. By performing a cross-correlation analysis between the time-series of 427.8 nm ($N_2^+$ first negative band) and 557.7 nm oxygen emissions, they derived the distribution of the lifetime of O($^1$S). The mean of the lifetime is 0.67 s and the mode is around 0.7 s. They estimated the emission altitude of PsA using the lifetime of O($^1$S) and then carried out a case study, in which they compared the temporal variations of the emission altitude with the peak height of E-region ionisation obtained from the simultaneous observation of the EISCAT UHF radar (Figure 6). They confirmed an overall agreement between the two parameters, indicating the feasibility of using the current method for estimating the energy of precipitat-

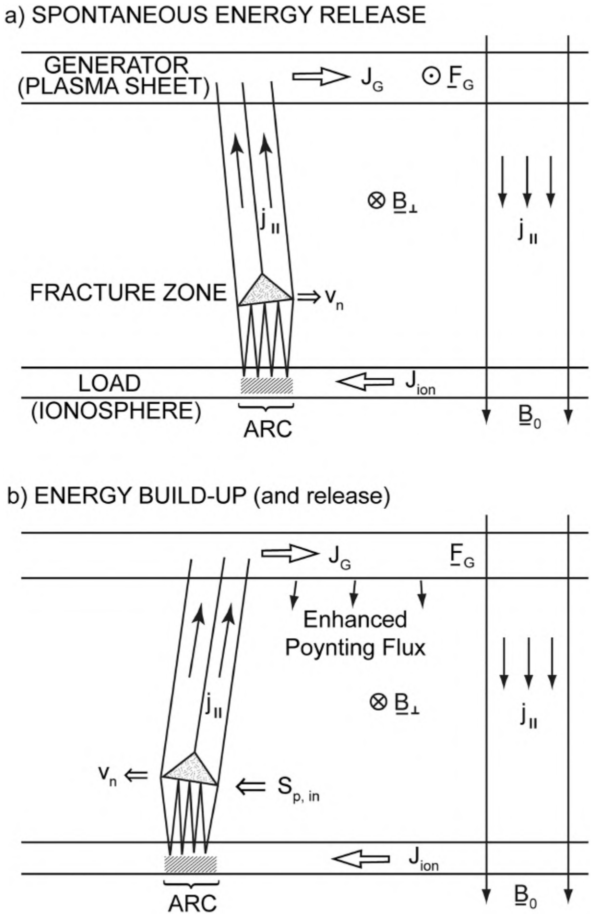

Figure 5: Illustration of two types of auroral arcs, distinguished by the way they propagate (velocity $v_\mathrm{n}$) with respect to the interior of the associated current circuit (Field-aligned currents: $j_\parallel$, and open arrows for generator and ionospheric closure currents. $\underline{F}_\mathrm{G}$ = generator force). In case (a) the arc is powered from above by the release of shear stresses, in case (b) it is powered from the interior of the current circuit ($S_\mathrm{p,in}$) and one half of the energy is invested in shearing the field of the newly incorporated magnetic flux.

ing electrons causing PsA. In addition, they derived the statistical characteristics of the emission altitude of PsA. The result shows that the emission altitude becomes lower in the morning side than in the midnight sector, which indicates that the energy of PsA electrons is higher in the later MLT sector. Especially, there is a decrease of the emission altitude at around 06 MLT. However, the model calculation infers that the energy of cyclotron resonance between magnetospheric electrons and whistler-mode chorus waves does not change so much depending on MLT. This implies that the observed change of the emission altitude cannot be explained only by the MLT dependence of resonance energy.

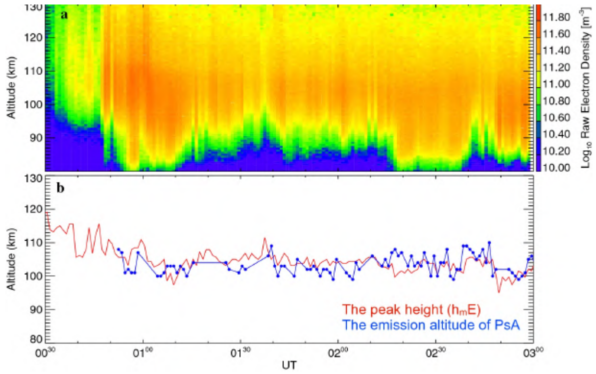

Figure 6: (a) Altitude-time plot of the ionospheric raw electron density (i.e., power profile data) obtained by the EISCAT UHF radar for an interval of pulsating aurora from 00:30 UT to 03:00 UT on 19 February 2018. (b) Time-series of the emission altitude of pulsating aurora estimated from the lifetime of $\mathrm{O}(^1\mathrm{S})$ (blue line) and the peak height of E-region ionisation ($h_\mathrm{m}E$) from EISCAT (red line).

## High-resolution optical observations of neutral heating associated with the electrodynamics of an auroral arc

Price et al. (2019) used data from the Auroral Structure and Kinetics (ASK) instrument on Svalbard to measure the atmospheric neutral temperature profile, over auroral altitudes, at unprecedented temporal and spatial scales. EISCAT Svalbard radar (ESR) data were used to constrain estimates of the electron density from the Southampton electron transport and ion chemistry model, in order to extract neutral temperatures (Figure 7).

## Studies of polar cap patches and throat aurora

Jin, Xing et al. (2019) performed a statistical analysis of 345 polar cap patches at the dayside sectors during 09:00–15:00 magnetic local time, observed by EISCAT Svalbard Radar. The results show that the polar cap patches are preferentially formed during southward IMF conditions. Moreover, the results indicate that the pulsed dayside magnetic reconnection is possibly a significant formation mechanism of polar cap patches.

An EISCAT Svalbard Radar campaign was run together with with all-sky cameras. Han et al. (2019) observed the spatio-temporal evolution of

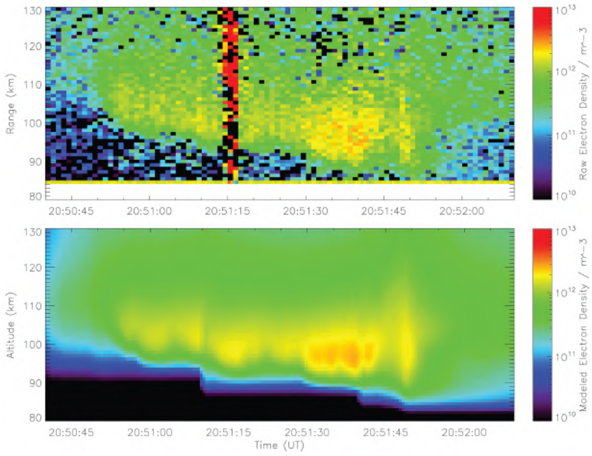

Figure 7: Comparison between the observed raw electron density from the EISCAT Svalbard Radar (top panel) and the corresponding modelled electron density from the University of Southampton ion chemistry and electron transport model (bottom panel). The large red artefact visible in the ESR power profiles is a result of a poor fit in the analysis software and was ignored in the analysis.

flow reversals, Joule heating as well as ion upflows associated with throat aurora for the first time (Figure 8). These results are consistent with the geometry of the flux transfer event model devised by Southwood in 2007, and provide strong evidence for throat aurora being associated with magnetopause reconnection events. The results also support a conceptual model of the throat aurora.

# Studies of the ionosphere

## Plasma density gradients at the edge of polar ionospheric holes: the absence of phase scintillation

Jenner et al. (2020) used the EISCAT Svalbard radar in conjunction with GNSS measurements to observe polar holes close to the Northern Hemisphere winter solstice in 2014 and 2015 (Figure 9), during geomagnetically quiet conditions. The expected phase scintillation was not present, such that they could to conclude that significant electron density gradients and plasma density levels above a certain threshold are required for scintillation to occur.

## Characteristics of CME- and CIR-driven ion upflows in the polar ionosphere

Ogawa et al. (2019) investigated how velocity and flux of ionospheric ion up-flows vary during magnetic storms driven by co-rotating interaction regions (CIRs) and coronal mass ejections (CMEs), using data from the European Incoherent Scatter (EISCAT) Tromsø UHF and Svalbard radars between 1996 and 2015. The characteristics of ion up-flows were compared with ion and electron temperature variations measured with the EISCAT radars and also Joule heating rate, electric field, and field-aligned current distribution derived from the Weimer model. Upward ion velocity increases in the night-time at Tromsø (66.2° N geomagnetic latitude) just after the CIR- and CME-driven storms, corresponding to electron temperature enhancements due to soft particle precipitation and also ion temperature enhancements in the strong westward electric field region. The CME-driven storms have larger upward ion flux (around $1.7 \times 10^{13}\,\mathrm{m^{-2}\,s^{-1}}$) than those under the CIR-driven storms (around $0.3 \times 10^{13}\,\mathrm{m^{-2}\,s^{-1}}$). In the daytime, ion up-flows are seen at Longyearbyen, Svalbard (75.2° N geomagnetic latitude), with an upward flux of typically $10^{13}\,\mathrm{m^{-2}\,s^{-1}}$ for small CIR and CME storm cases (Figure 10). Substantial ion upflows last for a few days after the storm onsets under small CIR storms, whereas they last for only a day under small CME storms. Under both the cases, the substantial ion upflows are associated with an enhancement of the Region 1 field-aligned current, eastward electric field and Joule heating rate. For large CME storms, substantial ion upflows are absent in the daytime probably due to equatorward expansion of the auroral oval.

## High-latitude crochet: solar-flare-induced magnetic disturbance independent from low-latitude crochet

A solar-flare-induced, high-latitude (peak at 70° to 75° geographic latitude, GGlat) ionospheric current system was studied by Yamauchi et al. (2020). Right after the X9.3 flare on 6 September 2017, magnetic stations at 68° to 77° GGlat near local noon detected northward geomagnetic deviations ($\Delta B$) for more than 3 h, with peak amplitudes of more than 200 nT without any accompanying substorm activities. From its location, this solar flare effect, or crochet, is different from previously studied ones, namely, the subsolar crochet (seen at

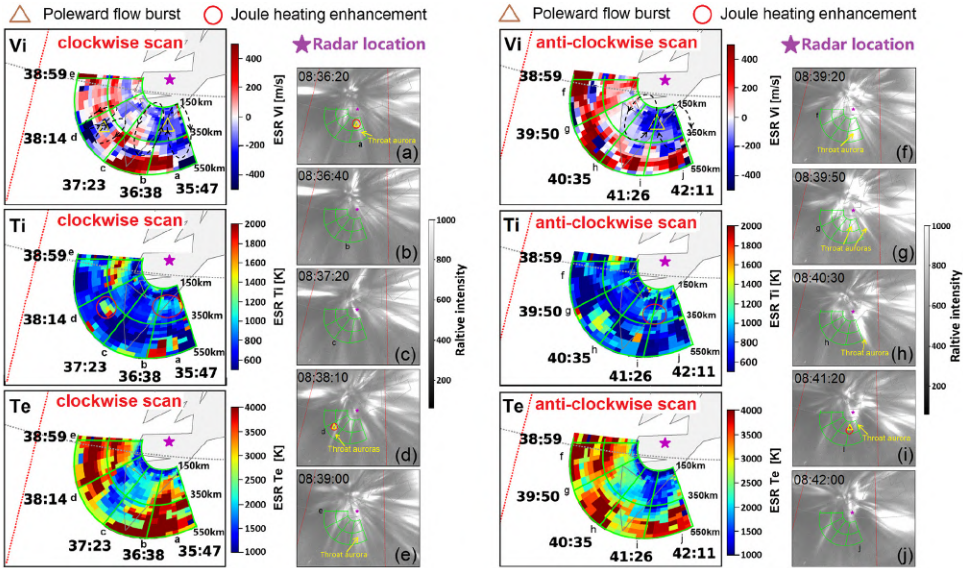

Figure 8: Two EISCAT Svalbard Radar 32 m antenna scans of $V_\mathrm{i}$, $T_\mathrm{i}$, and $T_\mathrm{e}$ from 08:35:47 to 08:42:11 UT on 28 November 2017 are compared to auroral observations. The radar and optical observations for the clockwise/counterclockwise scan are shown in the left/right two columns, respectively. The purple pentagons indicate the location of the ESR site. The fan-shaped grids show the coverage of the 32 m radar beam in the altitude range of 150 km to 550 km. The letters "a" to "j" shown at the bottom of the fan-shaped grid indicate the approximate directions of the radar beam at the time of the auroral images (a) to (j). The capture time of each auroral image is given in the top left corner on the image, and the throat auroras are indicated in yellow text. Yellow triangles inside the two $V_\mathrm{i}$ panels indicate anti-sunward flow bursts and are overlaid with the auroral images for easier comparison. Red circles in the $T_\mathrm{i}$ observations indicate some Joule heating events associated with the anti-sunward flow bursts, which are overlaid with the aurora images for easier comparison. In the $V_\mathrm{i}$ observations, Han et al. (2019) infer mesoscale flow cells that highlighted by black dashed circles with arrows.

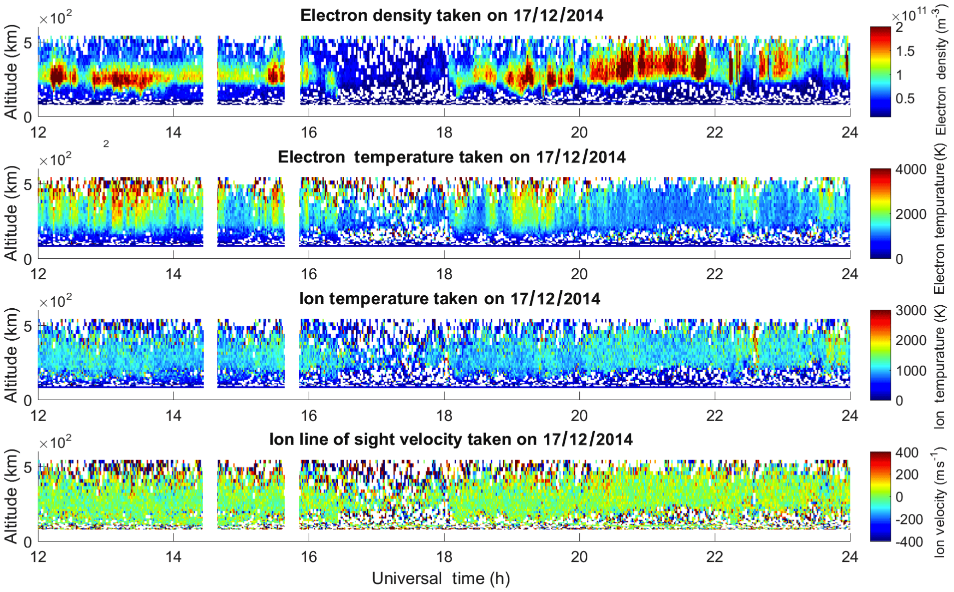

Figure 9: Electron densities, electron temperatures, ion temperatures, and ion drift line-of-sight velocity measured by the 42 m dish of ESR observing at an azimuth of 184.5° and an elevation of 81.6° between 12:00 and 23:59 UT on 17 December 2014.

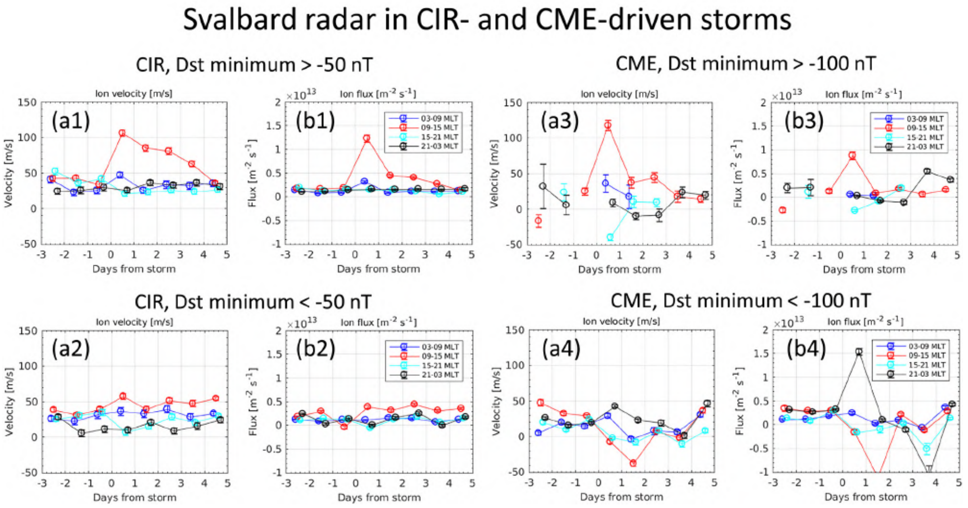

Figure 10: Averaged velocity and flux of up-flowing ions measured with the EISCAT Svalbard radar. In these plots, averaged values at 3 to 9, 9 to 15, 15 to 21 and 21 to 3 MLT are plotted with blue, red, cyan, and black colours, respectively. They are divided into four categories: (a1 and b1) CIR-driven small storms (Dst minimum $>-50$ nT), (a2 and b2) CIR-driven large storms (Dst minimum $<-50$ nT), (a3 and b3) CME-driven small storms (Dst minimum $>-100$ nT), and (a4 and b4) CME-driven large storms (Dst minimum $<-100$ nT). (CIR is co-rotating interaction region; CMEis coronal mass ejection; MLT is magnetic local time.)

lower latitudes), auroral crochet (pre-requires auroral electrojet in sunlight), or cusp crochet (seen only in the cusp). The new crochet is much more intense and longer in duration than the subsolar crochet. The long duration matches with the period of high solar X-ray flux (more than M3-class flare level). Unlike the cusp crochet, the interplanetary magnetic field (IMF) $B_Y$ is not the driver, with the $B_Y$ values of only 0 nT to 1 nT out of a 3 nT total field. The equivalent ionospheric current flows eastward in a limited latitude range but extended at least 8 h in local time (LT), forming a zonal current region equator-ward of the polar cap on the geomagnetic closed region.

EISCAT radar measurements (Figure 11), which were conducted over the same region as the most intense $\Delta B$, show enhancements of electron density (and hence of ion-neutral density ratio) at these altitudes (around 100 km) at which strong background ion convection (larger than 100 m s$^{-1}$) pre-existed in the direction of tidal-driven diurnal solar quiet (Sq0) flow. Therefore, this new zonal current can be related to this Sq0-like convection and the electron density enhancement, for example, by descending the E-region height. However, Yamauchi et al. (2020) have not found why the new crochet is found in a limited latitudinal range, and therefore, the mechanism is still unclear compared to the subsolar crochet that is maintained by a transient redistribution of the electron density.

The signature is sometimes seen in the auroral electrojet (AE $=$ AU $-$ AL) index. A quick survey for X-class flares during solar cycle 23 and 24 shows clear increases in AU for about half the flares larger than X2 during non-substorm time, despite the unfavourable latitudinal coverage of the AE stations for detecting this new crochet. Although some of these AU increases could be the auroral crochet signature, the high-latitude crochet can be a rather common feature for X flares.

1. A new type of the solar flare effect on the dayside ionospheric current at high latitudes but equatorward of the cusp during quiet periods was found.
2. The effect is also seen in the AU index for nearly half of the larger than X2-class solar flares.
3. A case study suggests that the new crochet is related to the Sq0 (tidal-driven part) current.

## Multi-instrument observations of ion-neutral coupling in the dayside cusp

Billett et al. (2020) used data multiple data sources, including the EISCAT Svalbard radar, to examine

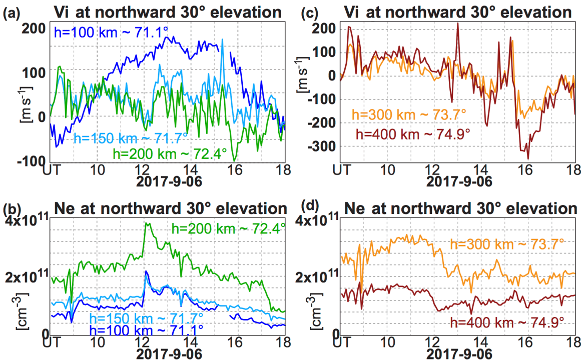

Figure 11: Ionospheric line-of-sight ion velocity and electron density observed by EISCAT Tromsø VHF (224 MHz) radar from 69° GGlat, looking northward at its lowest elevation angle (30°) above the horizon. Panels (a) and (c) show the ion velocity, and panels (b) and (d) show the electron density.

an instance of F-region neutral winds influenced by the presence or poleward moving auroral forms near the dayside cusp (Figure 12). They observed a reduction in the time taken for the ion drag force to re-orientate the neutrals into the direction of the convective plasma (on the order of minutes), compared to before the auroral activity began. Neutrals were observed responding to an interplanetary magnetic field change within minutes of it occurring. This has implications on the rate that energy is deposited into the ionosphere via Joule heating.

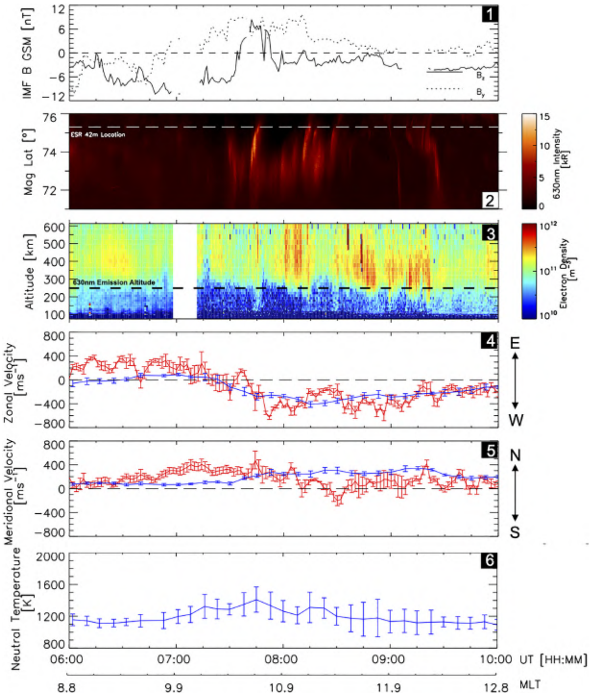

Figure 12: Overview of the 8 December 2013 event. 1: The interplanetary magnetic field $B_z$ and $B_y$ components (OMNI data set, lagged to the dayside ionosphere). 2: Auroral 630 nm intensity keogram (Svalbard all-sky imager). 3: Altitude-time plot of the electron density (ESR 42 m beam). 4: Average zonal and 5: meridional velocity components of the neutrals (blue, SCANDI) and plasma (red, SuperDARN). 6: Average neutral temperatures from SCANDI. The zonal and meridional velocities and the neutral temperatures are averages between 71° and 76° magnetic latitude within the SCANDI field of view. Error bars on 4, 5, and 6 are standard deviations.

## Studies of characteristics of polar mesospheric summer and winter echoes

The characteristics of polar mesospheric summer echoes (PMSE) modulated by HF heating was studied by Ullah et al. (2019). It was found that all the characteristics of modulated PMSE, except the PMSE recovery, are greater in the lower layer than in the upper layer. The enhanced electron temperature has significant effect on the PMSE modulation index, and further, the variability of electron temperature may be responsible for the variations in different modulated PMSE characteristics between the lower and upper layers.

The effect of high energy particle precipitation on PMSE intensity was investigated by Rauf, Hailong et al. (2019). The computed correlation between the high energy particle precipitation and PMSE shows that the variations in high energy particle precipitation and PMSE are positively correlated. The electron density irregularity caused by precipitating particles might be one of the possible reasons for this positive correlation. Moreover, K-indices and electron fluxes also support the observed positive correlation, whereas the X-rays and proton fluxes have no noticeable effect on PMSE.

In a study by Rauf, Li et al. (2019) the PMSE were mostly observed by the EISCAT UHF radar in the early morning and forenoon, and are positively correlated with Lyman-$\alpha$ radiation, suggesting that solar radiation might be important for those PMSE. Moreover, a study by Ge et al. (2019) found that the positive correlation between the variation in PMSE and noctilucent clouds (NLC) supports the earlier proposed idea about the role of ice particle in producing PMSE. Furthermore, the seasonal behaviour of PMSE was found by

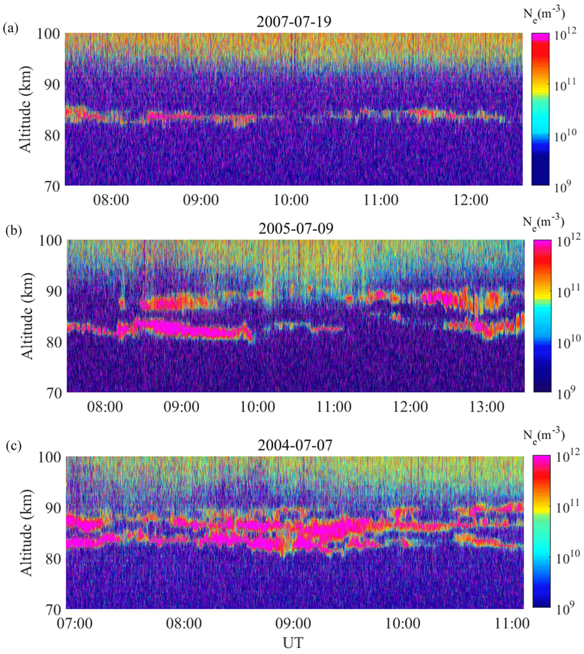

Figure 13: The typical layered PMSE events observed by EISCAT 224 MHz VHF radar. (a) Monolayer PMSE. (b) Double-layer PMSE. (c) Tri-layer PMSE.

analysing the seasonal variation of PMSE mono-, double-, and tri-layer occurrence ratio (Figure 13). A method was developed to calculate the PMSE mono-, double-, and tri-layer occurrence ratio under a different electron density threshold. In addition, a method to analyse the correlation of the layered PMSE occurrence ratio with the solar 10.7 cm flux index ($F10.7$) was proposed. The PMSE occurrence ratio was found to be positively correlated with the K-index, but only weakly with F10.7.

Ullah et al. (2020) used an analytical model to investigate modulated polar mesospheric winter echoes (PMWE) by introducing winter parameters. The important role of charged dust particles in the creation of PMWE was confirmed.

The frequency dependence of the volume reflectivity and the effect of energetic particle precipitation on modulated PMSE were investigated by Ge et al. (2020). It was shown that the high-frequency heating had a very limited impact on the PMSE when the electron density detected by the EISCAT UHF radar was enhanced by energetic particle precipitation. In addition, an updated qualitative method to study the relationship between volume reflectivity and frequency, was developed.

## On the production of ionospheric irregularities via Kelvin-Helmholtz instability associated with cusp flow channels

Spicher et al. (2020) combine EISCAT Svalbard radar (ESR) data with GNSS (Global Navigation Satellite Systems), SuperDARN (Super Dual Auroral Radar Network) and DMSP data to investigate phase scintillations associated with enhanced flow channels of F-region ionospheric plasma. Phase scintillations of radio signals used by GNSS occur as the signal passes through the turbulent ionospheric region and can cause problems for the system. At high latitudes, this ionospheric turbulence has a number of sources, one of which is presented in this paper: A Kelvin Helmholtz instability (KHI) which develops at a flow shear boundary within the ionosphere (such as those as the edges of flow channels). Whilst SuperDARN provided observations of the large scale (on the order of 10 km) ionospheric convection, the ESR (32 m dish operating in an azimuthal scan "windscreen wiper" mode at 30° elevation) provided observations of the meso- and small-scale (on the orders 10 m to 100 m) flow channels associated with the scintillations. The authors presented evidence of strong phase scintillations ($\sigma_\phi$ larger than 0.5 rad) associated with a region of sheared flow with structured low-energy particle precipitation (see Figure 14). To strengthen the observations, a quantitative, non-linear analysis of the KHI and its impact on phase scintillations was undertaken using numerical simulations from GEMINI (Geospace Environment Model of Ion-Neutral Interactions) — SIGMA (Satellite-beacon Ionospheric Scintillation Global Model of the Upper Atmosphere). Using data from the ESR as input to the simulation the authors found that the KHI could efficiently create the required turbulence (see Figure 15). The authors point out the potential that an incoherent scatter radar with a wide field of view capability will have great potential for investigating such phenomena in the future.

# Active experiments

## Experimental results from ionospheric heating

The intensities in high frequency-enhanced ion lines (HFIL, Figure 16) and high frequency-enhanced plasma lines (HFPL, Figure 17) excited by powerful pumping were examined by J. Wu et al. (2019), and an alternative explanation for

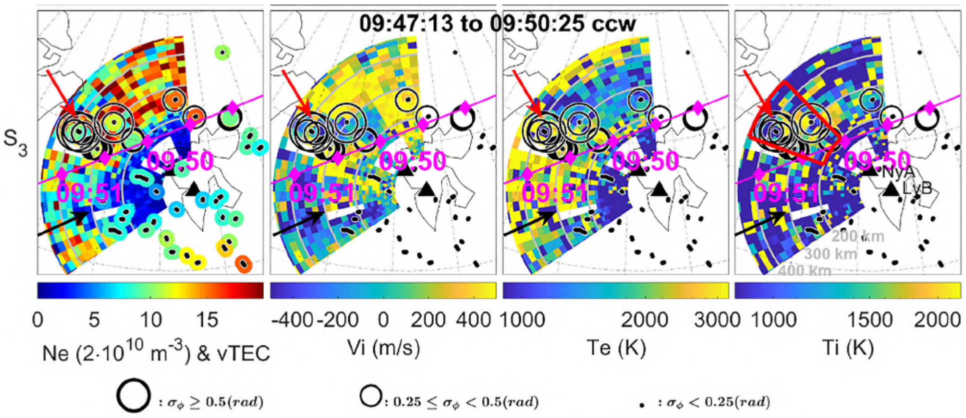

Figure 14: An ESR fan plot showing, from left to right, ionospheric electron density, line-of-sight ion velocity, electron temperature and ion temperature. The time taken to complete the scan was 192 s (from 09:47:13 to 09:50:25) with the dish moving in a counter clockwise (CCW) direction. The vertical TEC (total electron content) is shown super-imposed on the electron density scan, using the same colour scale. The amount of phase scintillation observed at each of the ionospheric piercing points is shown by the small, medium and large circles (using the scale beneath the panels. The pink line marks the footprint of the overpassing DMSP-17 satellite. The red and black arrows highlight regions of interest with the red box indicating the region with the largest phase scintillation.

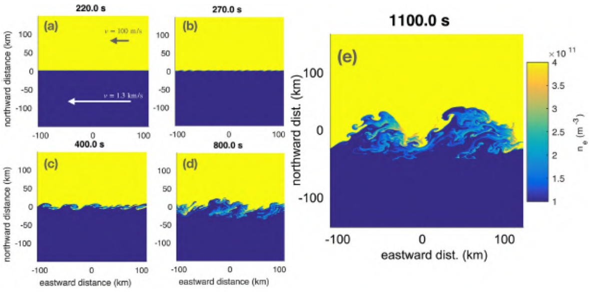

Figure 15: Snapshots from the numerical simulation showing the electron density from GENINI at 300 km altitude at different times during the development of the KHI.

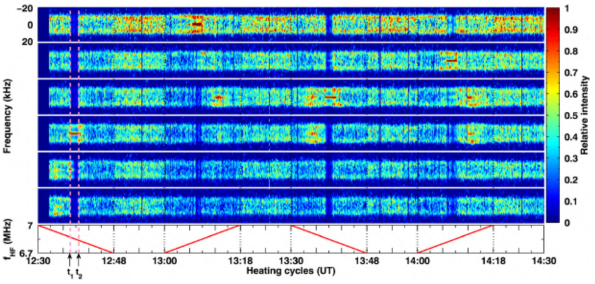

Figure 16: (From top to bottom) The normalised ion line at the altitudes 215.43 km, 212.5 km, 209.57 km, 206.63 km, 203.7 km and 200.77 km versus the heating cycles (bottom panel).

overshoot in HFIL and HFPL was presented. The study showed that the enhanced electron temperature plays a significant role in the intensities of HFIL and HFPL, that is, the enhanced electron temperature may modify the wave number of the enhanced Langmuir and ion acoustic waves. Furthermore, it was noted that the overshoot could be attributed to the enhancement in electron temperature on the travelling path.

A number of heating experiments were examined by Feng et al. (2020). An experiment using cold-start X-mode heating showed generation of parametric decay instability while no overshoot was observed. During other experiment using power-stepped X-mode heating with noticeable O-mode wave leakage, the parametric decay instability and the oscillating two-stream instability were generated at the O-mode reflection height without the overshoot effect. It was proposed that the electron temperature increased because the X-mode heating below the upper-hybrid height decreased the growth rate of the thermal parametric instability.

## The 3-D distribution of artificial aurora induced by HF radio waves in the ionosphere

Kvammen et al. (2019) looked at 3-D excitation rate estimates of artificial aurora in the ionospheric F layer, induced by the EISCAT heater. The authors used multi-station optical observations of three different enhanced Oxygen emission lines (6300 Å, 5577 Å and 8446 Å) using ALIS (Auroral

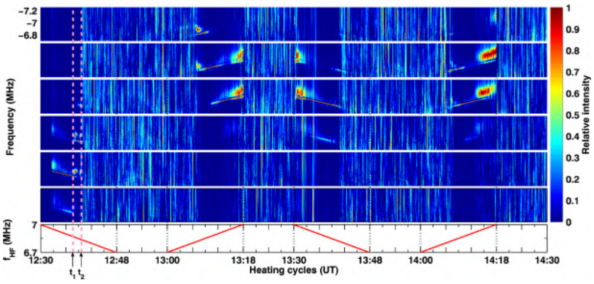

Figure 17: From top to bottom) The normalised plasma line at the altitudes 210.25 km, 207.32 km, 204.39 km, 201.45 km, 198.52 km and 195.58 km versus the heating cycles (bottom panel), where $t_1$ and $t_2$ are the same as in Figure 16.

Large Imaging System) at four different locations (Abisko, Kiruna, Silkimuotka, and Tjautjas) to test predicated excitation-altitude profiles, calculated using the method described in 2008 by Gustavsson and Eliasson. This was the first time that four imaging stations in the 6300 Å and 5577 Å emission lines have been used in 3-D artificial auroral reconstruction and the first estimates of the 8446 Å emission line volume distribution. An exposure time of 6 s was chosen at all ALIS stations and for all emission line filters, providing images approximately every 10 s. The EISCAT heater was used in a 150 s heating on and 85 s heating off cycle modulation, making it possible to measure the sky background between the heating pulses and to estimate the decay time of the 6300 Å emission. The EISCAT UHF radar was operated with a meridional scan pattern, providing plasma parameter measurements of the heated volume with approximately 3 km altitude resolution and 5 s time resolution. The electron temperature was enhanced to approximately 3300 K (2500 K) at the resonance height during 6.2 MHz (5.423 MHz) heating.

Figure 18 shows the UHF electron temperature observations and the enhanced emission intensities at the four different locations and three different emission lines. The light grey boxes represent heating on during 6.2 MHz pumping and the dark grey boxes heating on at 5.423 MHz pumping. The enhancements in the intensity of the 6300 Å observations are not synchronized to the pump periods due to the long $O(^1D)$ lifetime. The scanning of the UHF beam through the heated volume is represented by the red line in the electron temperature panel. The 3-D artificial aurora reconstruction was achieved by adjusting a 3-D parametrised aurora model so that the model projections fitted the observed images. The 3-D aurora models were constructed with a two-dimensional Gaussian in the horizontal plane combined with three different profiles along the magnetic field: (1) Gaussian distribution, (2) Gustavsson-Eliasson profiles, and (3) modified Gustavsson-Eliasson profiles. The paper noted that the 3-D reconstructions suggests that the distribution of energised electrons is less extended in altitude than predicted by transport calculations of electrons accelerated to 2 eV to 100 eV. After considering different explanations for this they concluded that a possible reason for this discrepancy is that high-frequency pumping might induce an anisotropic distribution of energized electrons whereas the Gustavsson-Eliasson model assumes isotropic distributions.

## ELF and VLF waves excited by HF pumping

Comparing the dependence of extremely/very low frequency (ELF/VLF) radiation excited by amplitude modulation (AM) and dual-beam beat-wave (BW) mode modulation on the geomagnetic field disturbance, it was shown by Yang et al. (2019) that in quiet geomagnetic condition, heating increases and the ionisation of the lower ionosphere decreases in BW. The result seems to support that BW heating is mainly due to the ponderomotive non-linearity located in the ionospheric F layer.

However, the correlation coefficient between VLF amplitude and the deviation of the geomagnetic north-south component, as studied by Ma, Guo, Yang et al. (2019), illustrates that strong and positive correlation occurs more frequently than the negative correlation, which supports that VLF by BW is excited in the D or E region. Furthermore, a polarisation analysis of BW-generated ELF/VLF, performed by T. Xu et al. (2019), showed that ELF/VLF can be decomposed into right- and left-handed circularly polarised waves with comparable strengths, and that the polarisation ellipse tends to be parallel to the well-known dominant background electric field. This is consistent with the recognized features of ELF/VLF generated by modulation of the polar electrojet current taking place in the D and E regions.

ELF waves excited by the EISCAT heater were received by the electric field detector on the China seismo-electromagnetic satellite (CSES) in a study by Yang et al. (2020). It was observed that although the ELF intensity excited by beat-wave modulation (BW) was far lower than that in amplitude modulation (AM) on the ground, the ratio of ELF

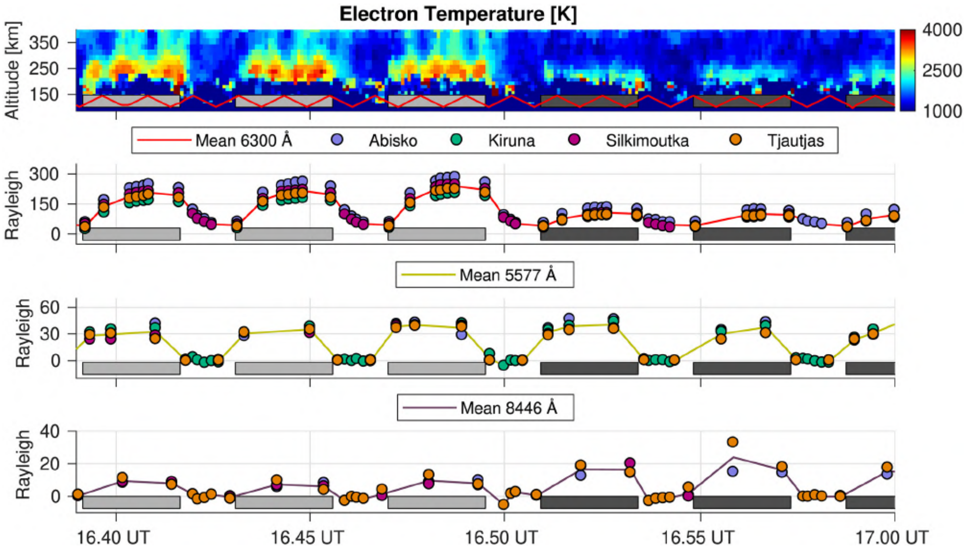

Figure 18: UHF electron temperature observations and the enhanced emission intensities. The light gray boxes represent heating on during 6.200 MHz pumping and the dark gray boxes heating on at 5.423 MHz pumping. $I_{6300}$ is not synchronized to the pump periods due to the long $O(^1D)$ lifetime. The scanning of the UHF beam through the heated volume is represented by the red line in the electron temperature panel.

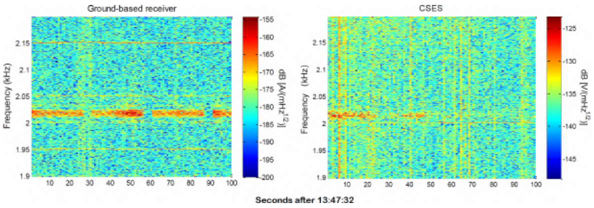

Figure 19: Signals received from the ground-based receiver and the CSES receiver in the ELF communication experiment by modulated heating.

intensities between the satellite and the ground in BW was significantly larger than that in AM.

Lu et al. (2021) showed that CSES additionally received VLF signals during the first ELF/VLF communication experiments conducted using the EISCAT heater. This implies that the ELF/VLF excited by amplitude modulation heating of the auroral electrojet can be used for long-distance communication (Figure 19).

## Electron heating by HF pumping of high-latitude ionospheric F-region plasma near magnetic zenith

High-frequency electromagnetic pumping of ionospheric F-region plasma at high and mid latitudes gives the strongest plasma response in magnetic zenith, anti-parallel to the geomagnetic field in the northern hemisphere. This has been observed in optical emissions from the pumped plasma turbulence, electron temperature enhancements, filamentary magnetic field-aligned plasma density irregularities, and in self-focusing of the pump beam in magnetic zenith. Leyser et al. (2020) present results of EISCAT (European Incoherent SCATter association) Heating-induced magnetic-zenith effects observed with the EISCAT UHF incoherent scatter radar. With heating transmitting a left-handed circularly polarized pump beam towards magnetic zenith, the UHF radar was scanned in elevation in steps of 1.0° and 1.5° around magnetic zenith. The electron energy equation was integrated to model the electron temperature and associated electron heating rate and optimized to fit the plasma parameter values measured with the radar. The experimental and modelling results are consistent with pump wave propagation in the L mode in magnetic zenith, rather than in the O mode. See Figure 20.

## Stimulated electromagnetic emissions

With the EISCAT HF-transmitter at the heating facility running in X mode, a narrow continuum in the stimulated electromagnetic emission (SEE) spectrum occurs under cold-start condition and shows an overshoot effect lasting several seconds. The cascading peaks occur on both sides of the heating frequency only in the preconditioned ionosphere and are also showing an over-

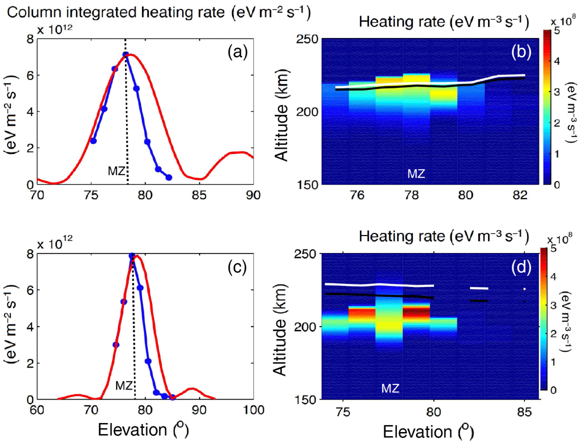

Figure 20: Modelled electron heating rate $Q_{\mathrm{HF}}$ ($\mathrm{eV\,m^{-3}\,s^{-1}}$) during steady state versus radar elevation angle for 25 November 2014 (a, b) and 24 October 2017 (c, d). Panels a and c display the column-integrated $Q_{\mathrm{HF}}$ (blue dots, with connecting lines to guide the eye) and the relative intensity of the transmitted Heating beam (red) assumed to propagate in vacuum. The elevation corresponding to magnetic zenith is indicated by the dashed line and labelled MZ. Panels b and d show the altitude profiles of $Q_{\mathrm{HF}}$. The white line indicates the altitude of the plasma resonance where $f_p = f_0$ and the black line shows the upper hybrid resonance height at which the upper hybrid frequency equals $f_0$. Note that the elevation scale is different in panels a and b and c and d.

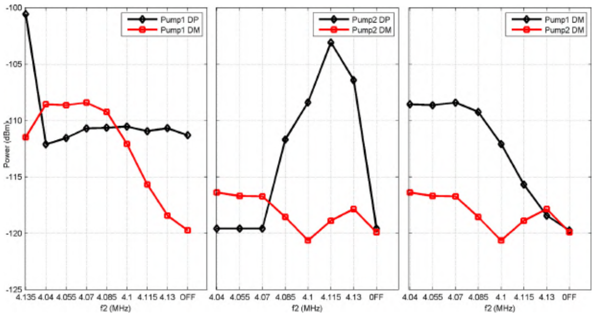

Figure 21: Variations in power of the DP and DM of the two pump waves along with $f_2$ frequency. (a) DM and DP of pump wave 1; (b) DM and DP of pump wave 2; (c) DM of the two pump waves.

shoot. Wang et al. (2019) concluded that these SEE features are probably related to the ponderomotive force.

An ionospheric heating campaign was carried out by operating two-pump wave ionospheric heating at frequencies $f_1$ and $f_2$ respectively, where $f_1 < f_2$. Observations by Ma, Guo, Li et al. (2019) and Lv et al. (2019) show that when the pump wave at $f_2$ was on, the down-shifted peak (DP) power of $f_1$ decreased, whereas the down-shifted maximum (DM) of $f_1$ was further enhanced (Figure 21), which may be due to the gyro-resonance at the upper hybrid altitude. Additionaly, it took less than 10 s to reach a steady state for DP, which was nearly consistent with the growth time of the small-scale artificially field-aligned irregularity. Thus, it may be deduced that the small-scale artificially field-aligned irregularity plays an important role in the DP generation process.

An experimental investigation of stimulated Brillouin scattering (SBS) features and electron temperature inversion near the third electron gyroharmonic $3f_{\mathrm{ce}}$, was performed by H. Y. Fu et al. (2020). The evolution of the SBS features varies asymmetrically near $3f_{\mathrm{ce}}$, and the asymmetries among SBS, electron temperature, and the high frequency pump enhanced ion line (HFIL) are clearly exhibited for pumping above $f_0 \geq 3f_{\mathrm{ce}}$. The electron temperature at the resonance regime was retrieved from the measured SBS spectra based on the wave matching theory. The inversion results by SBS are consistent with measurements made by the EISCAT UHF incoherent scatter radar at the resonance altitude.

# Methods and modelling

## Statistical modelling of the coupled F-region ionosphere-thermosphere at high latitude during polar darkness

Dorrian et al. (2019) used data from the EISCAT Svalbard radar together with measurements from a co-located Fabry-Perot Interferometer to develop statistical models for predicting the behaviour of the coupled high-latitude ionosphere-thermosphere system. They modelled the F-layer peak electron density, plasma structuring, ion temperature, neutral temperature, and the difference between these temperatures (Figure 22). Multivariate models were developed showing the combinations of parameters that best explained the observed variability. A comparison with climatology showed that the models give an improvement in every case with skill scores based on the mean square error of up to 0.88.

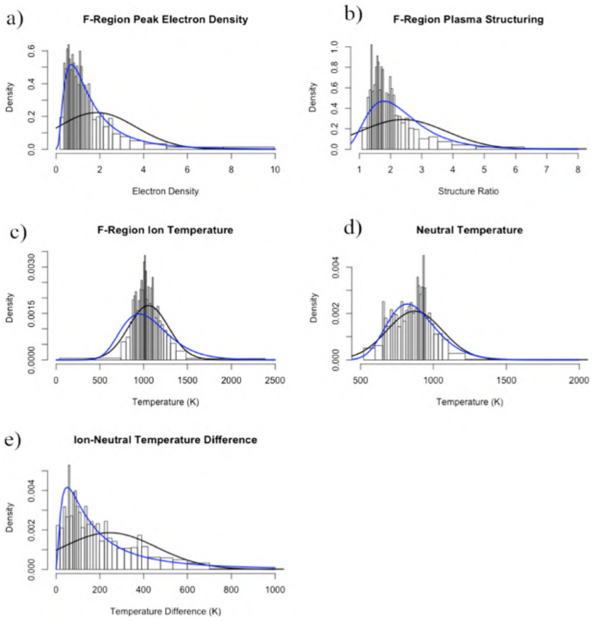

Figure 22: Panels a to e show histograms and fitted distribution curves for the data for $F_{\mathrm{Ne}}$, $F_{\mathrm{str}}$, $T_{\mathrm{i}}$, $T_{\mathrm{n}}$, and $T_{\mathrm{i}} - T_{\mathrm{n}}$, respectively. Black is normal, and blue is log-normal. For all dependent variables except $T_{\mathrm{i}}$, it was found that a log-normal distribution was the best fit to the data.

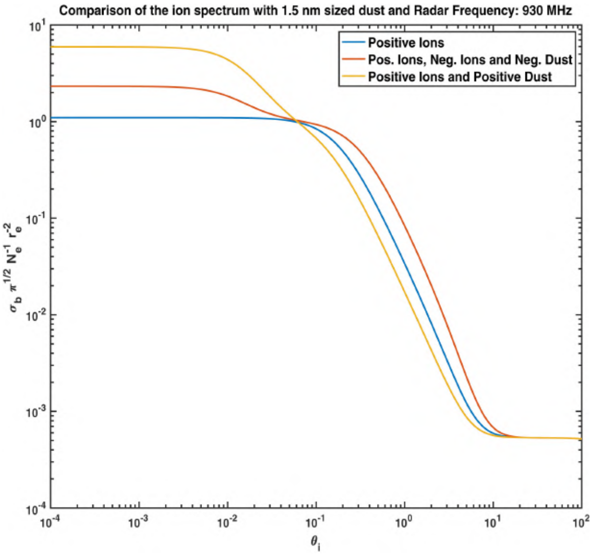

Figure 23: Ion line of the radar incoherent scatter spectrum in the presence of 1.5 nm charged dust. Calculations are for 930 MHz radar frequency.

## Radar studies of ionospheric dust-plasma phenomena

Mann et al. (2019) discuss the influence of charged dust on incoherent scatter radar observations. Dust particles influence the charge balance, resulting in so called “dusty plasmas” in the lower ionosphere. Polar mesospheric echoes are an example of such dust-plasma interactions which are observed with radar. The formation of the polar mesospheric radar echoes involves neutral atmosphere dynamics, which is latitude dependent and it involves charged dust particles, especially icy dust that forms in the polar summer mesosphere. The paper discusses the effect of charged dust on the shape of the incoherent scatter ion line spectrum (since the signal is that of Thomson scattering off electrons, where the electrons are coupled to other charged components). The authors note that observations have rarely reported charged dust signatures in the incoherent scatter spectra before demonstrating that there is a good chance for doing so with improved observations. Figure 23 shows modelled ion line spectra for the EISCAT UHF with (orange line and yellow line) and without (blue line) the presence of 1.5 nm charged dust. The results show that incoherent scatter can possibly also be used to estimate the amount of charged dust in the direct vicinity of a meteor (a prime contributor of ionospheric dust).

## Step-by-step ionospheric assimilation based on ground-based and space-borne observations

A study by N. Fu et al. (2019) introduced a Kalman filtering assimilation model that considers the errors from differential code biases (DCB) of GPS/LEO satellites and GNSS stations. The assimilation results and reliability were verified by various types of data, coming from sources such as ionMap, ionosondes, EISCAT incoherent scatter radars, and the electron density profiles coming from COSMIC ionPrf (occultation data) (Figure 24).

## Ducting of incoherent scatter radar waves by field-aligned irregularities

Rietveld and Senior (2020) provide a qualitative explanation for the observed apparent electron density enhancements seen in the UHF data, when the dish is pointed field-aligned, during HF heating experiments. The enhancements appear above the HF reflection altitude and often extend to 400 km to 650 km (the observable limits of the UHF radar in a field aligned position). The ISR technique relies on the fact that

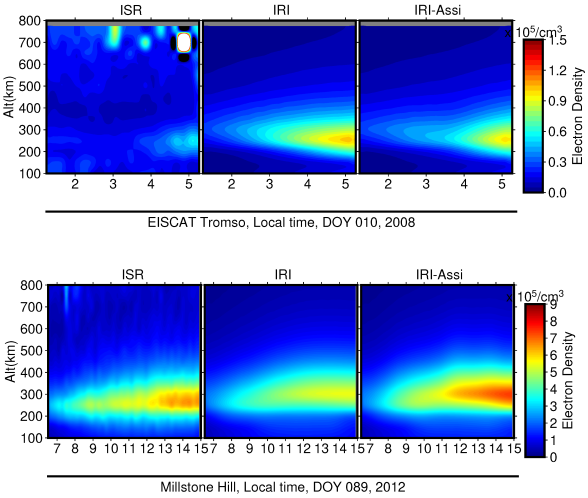

Figure 24: Densities measured by incoherent scatter radars compared to those coming from ionospheric models.

the ionospheric electron density is proportional to the backscattered power of the ion line. The authors revealed that the amount of power in the ion-line spectra was showing significant enhancements, which were being “incorrectly” interpreted by the analysis software as electron density enhancements. The authors named the enhancements WAILEs (Wide Altitude Ion Line Enhancements). Subsequent analysis also showed that the backscattered power in the plasma line spectra was also enhanced — indicating the effect is causing an increase the backscattered power at UHF frequencies from both ion-acoustic and Langmuir waves. Using a database of events from January 2001 until July 2018 they found 606 instances of WAILEs which occurred during both O- and X-mode heating. A simple ray-tracing model supports the suggestion that medium- to large-scale (tens to hundreds of metres) field aligned irregularities causes refraction leading to ducting of the radar waves along the magnetic field. As such, the amount of backscattered power received at the antenna is increased, which is interpreted as an enhancement in electron density.

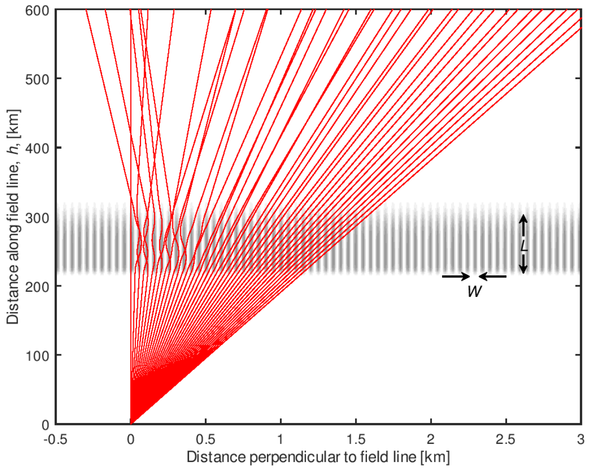

Figure 25: Ray paths of a set of 40 up-going 933 MHz waves from the transmitter at $(0, 0)$ with launch zenith angles evenly spaced between 0° and 0.3° passing through a region of vertically aligned irregularities, shown in grey, with horizontal wavelength, $W$ of 50 m and a length scale, $L$ of 80 km (extending from 220 km to 300 km altitude). The magnetic field-lines are assumed to be vertical. The rays illustrate the effects of refraction.

An example of this is shown in Figures 25 and 26, which illustrate the propagation paths of (a) up-going and (b) down-going waves at 933 MHz (the UHF frequency) antenna in the field aligned position. In Figure 25 it can be seen that the rays moving parallel to the field aligned irregularities (shown in grey at 220 km to 300 km) are refracted. In Figure 26 the downward propagation path (from one of the rays which arrived at 600 km in Figure 25) are shown and there is clear increase in the density of rays (backscatter power) near the receiver antenna. This mechanism also explains why the enhancements are not observed from the remote receiver sites (bi-static) since the scattering volume and angle between the receiver beam and the magnetic field aligned direction are larger. They point out that the excitation mechanism of the irregularities themselves remains poorly understood and thus represents an interesting research question in HF active experimental research. They also suggest that such ducting effects could also occurring under naturally occurring irregularities and that plasma line measurements should be used to determine the ionospheric electron density.

# EISCAT history

## Hunting the northern lights

As part of the JGR Space Physics Special Series *Pioneers of Space Physics*, Brekke (2020) was invited to provide a personal recollection of the early days of Chatanika and EISCAT. The article details the career of Professor Asgeir Brekke, from being sent, on a cargo ship, to Ny Ålesund, Svalbard, in the summer of 1966 as a newly qualified research as-

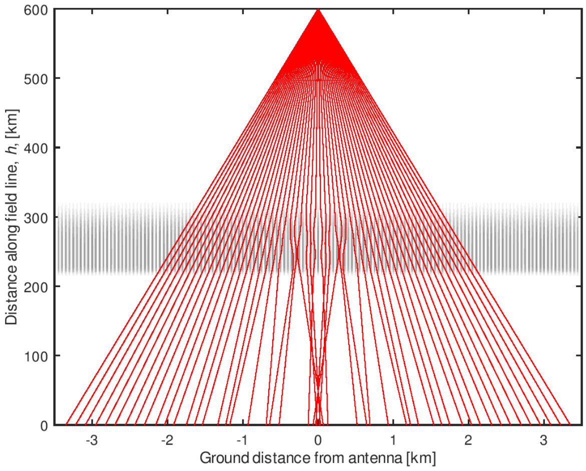

Figure 26: Backscattered, down-going 933 MHz rays from one of the up-going rays in Figure 25 which reached 600 km. The rays pass through the same irregularities as detailed in Figure 25. There is a clear increase in the density of the rays (backscattered power) near the receiver antenna at $(0,0)$, as well as regions of weaker backscatter further away.

Figure 27: Asgeir Brekke overlooking Kongsfjord from the top of Zeppelin mountain, Ny Ålesund.

sistant to help set up an auroral observatory to his instrumental work in setting up the EISCAT mainland and Svalbard radars and making EISCAT what it is today. It also includes his work in setting up the Charanika radar, in Alaska, in the early 1970s (redeployed to the auroral zone from the Pacific as it was "believed that the ionospheric disturbances formed there by nature closely resembled the ionospheric effects of atmospheric atomic bomb tests in the atmosphere"). In addition to the ground-breaking scientific highlights, it provides a fascinating insight into the people involved in not only the field of incoherent scatter theory and design, but also in Space Physics as a whole, from the late 1960s onwards. Many of the anecdotes involve people whose names will be familiar to any scientist working in the field (Alfvén, Schunk, Akasofu to name but a few). Figure 27 shows a young Brekke on top of Zeppelin mountain in Ny Ålesund, Svalbard. Figure 28 shows Brekke and the Norwegian minister for education, science and church, Professor Gudmund Hernes, unveiling the plaque at the proposed site for the newly funded EISCAT Svalbard Radar in May 1993.

Figure 28: Asgeir Brekke and Norwegian minister, Professor Gudmund Hernes, unveiling the plaque at the proposed site for the newly funded EISCAT Svalbard Radar in May 1993.

# Publications 2019–2020

Aruliah, A., Förster, M., Hood, R., McWhirter, I. & Doornbos, E. (2019). Comparing high-latitude thermospheric winds from Fabry-Perot interferometer (FPI) and challenging mini-satellite payload (CHAMP) accelerometer measurements. *Annales Geophysicae*, *37*(6), 1095–1120. https://doi.org/10.5194/angeo-37-1095-2019

Belakhovsky, V. B., Jin, Y. & Miloch, W. J. (2019). Influence of different ionospheric disturbances on the GPS scintillations at high latitudes. *Springer proceedings in Earth and environmental sciences* (pp. 281–287). Springer International Publishing. https://doi.org/10.1007/978-3-030-21788-4_24

Billett, D. D., Hosokawa, K., Grocott, A., Wild, J. A., Aruliah, A. L., Ogawa, Y., Taguchi, S. & Lester, M. (2020). Multi-instrument observations of ion-neutral coupling in the dayside cusp. *Geophysical Research Letters*, *47*(4), e2019GL085590. https://doi.org/10.1029/2019gl085590

Birch, M. J. & Hargreaves, J. K. (2020). Quasi-periodic ripples in high latitude electron content, the geomagnetic field, and the solar wind. *Scientific Reports*, *10*(1), 1313. https://doi.org/10.1038/s41598-019-57201-4

Blagoveshchenskaya, N. F. (2020). Perturbing the high-latitude upper ionosphere (F region) with powerful HF radio waves: A 25-year collaboration with EISCAT. *URSI Radio Science Bulletin*, *2020*(373), 40–55. https://doi.org/10.23919/ursirsb.2020.9318436

Blagoveshchenskaya, N. F., Borisova, T. D., Kalishin, A. S., Yeoman, T. K. & Häggström, I. (2020). Distinctive features of Langmuir and ion-acoustic turbulences induced by O- and X-mode HF pumping at EISCAT. *Journal of Geophysical Research: Space Physics*, *125*(7), e2020JA028203. https://doi.org/10.1029/2020ja028203

Blagoveshchenskaya, N. F., Borisova, T. D., Kalishin, A. S., Yeoman, T. K., Schmelev, Y. A. & Leonenko, E. E. (2019). Characterization of artificial, small-scale, ionospheric irregularities in the high-latitude F region induced by high-power, high-frequency radio waves of extraordinary polarization. *Geomagnetism and Aeronomy*, *59*(6), 713–725. https://doi.org/10.1134/s0016793219060045

Borisova, T. D., Blagoveshchenskaya, N. F., Kalishin, A. S., Häggström, M. I. & Rietveld, M. T. (2020). Excitation of Langmuir and ion-acoustic turbulence in the high-latitude ionosphere by a high-power HF radio wave simultaneously below and above the F2-layer maximum. *Radiophysics and Quantum Electronics*, *62*(12), 793–806. https://doi.org/10.1007/s11141-020-10025-z

Borisova, T. D., Blagoveshchenskaya, N. F., Rietveld, M. T. & Häggström, I. (2019). Outshifted plasma lines observed in heating experiments in the high-latitude ionosphere at pump frequencies near electron gyroharmonics. *Radiophysics and Quantum Electronics*, *61*(10), 722–740. https://doi.org/10.1007/s11141-019-09931-8

Bosse, L., Lilensten, J., Gillet, N., Rochat, S., Delboulbé, A., Curaba, S., Roux, A., Magnard, Y., Johnsen, M. G., Løvhaug, U.-P., Amblard, P.-O., Bihan, N. L., Nabon, M., Marif, H., Auriol, F. & Noûs, C. (2020). On the nightglow polarisation for space weather exploration. *Journal of Space Weather and Space Climate*, *10*, 35. https://doi.org/10.1051/swsc/2020036

Braun, V., Horstmann, A., Reihs, B., Lemmens, S., Merz, K. & Krag, H. (2019). Exploiting orbital data and observation campaigns to improve space debris models. *The Journal of the Astronautical Sciences*, *66*(2), 192–209. https://doi.org/10.1007/s40295-019-00155-6

Brekke, A. (2020). Hunting the northern lights. *Journal of Geophysical Research: Space Physics*, *125*(3), e2019JA027743. https://doi.org/10.1029/2019ja027743

Bruno, J., Mitchell, C. N., Bolmgren, K. H. & Witvliet, B. A. (2020). A realistic simulation framework to evaluate ionospheric tomography. *Advances in Space Research*, *65*(3), 891–901. https://doi.org/10.1016/j.asr.2019.11.015

Cai, L., Oyama, S., Aikio, A., Vanhamäki, H. & Virtanen, I. (2019). Fabry-Perot interferometer observations of thermospheric horizontal winds during magnetospheric substorms. *Journal of Geophysical Research: Space Physics*, *124*(5), 3709–3728. https://doi.org/10.1029/2018ja026241

Candela, L., Stocker, M., Häggström, I., Enell, C.-F., Vitale, D., Papale, D., Grenier, B., Chen, Y. & Obst, M. (2020). Case study: ENVRI science demonstrators with D4Science. *Lecture notes in computer science* (pp. 307–323). Springer International Publishing. https://doi.org/10.1007/978-3-030-52829-4_17

Chang, O., Bisi, M. M., Aguilar-Rodriguez, E., Fallows, R. A., Gonzalez-Esparza, J. A., Chashei, I. & Tyul'bashev, S. (2019). Single-site IPS power spectra analysis for space weather products using cross-correlation function results from EISCAT and MERLIN IPS data. *Space Weather*, *17*(7), 1114–1130. https://doi.org/10.1029/2018sw002142

Dalipi, B., Syla, N. & Aliaj, F. (2020). Electron temperature fluctuations on the eve and after the NEIAL events observed with the EISCAT Svalbard radar. *Acta Physica Polonica A*, *137*(4), 509–512. https://doi.org/10.12693/aphyspola.137.509

Danilov, A. D. & Konstantinova, A. V. (2020). Long-term variations in the parameters of the middle and upper atmosphere and ionosphere (review). *Geomagnetism and Aeronomy*, *60*(4), 397–420. https://doi.org/10.1134/s0016793220040040

Dorrian, G. D., Wood, A. G., Ronksley, A., Aruliah, A. & Shahtahmassebi, G. (2019). Statistical modeling of the coupled F-region ionosphere-thermosphere at high latitude during polar darkness. *Journal of Geophysical Research: Space Physics*, *124*(2), 1389–1409. https://doi.org/10.1029/2018ja026171

Feng, T., Zhou, C., Wang, X., Liu, M. & Zhao, Z. (2020). Evidence of X-mode heating suppressing O-mode heating. *Earth and Planetary Physics*, *4*(6), 1–10. https://doi.org/10.26464/epp2020068

Fu, H. Y., Jiang, M. L., Wang, K. N., Wu, J., Li, Q. L., Rietveld, M. T., Varberg, E., Häggström, I. & Jin, Y.-Q. (2020). Electron temperature inversion by stimulated Brillouin scattering during electron gyroharmonic heating at EISCAT. *Geophysical Research Letters*, *47*(17), e2020GL089747. https://doi.org/10.1029/2020gl089747

Fu, N., Guo, P., Wu, M., Huang, Y., Hu, X. & Hong, Z. (2019). The two-parts step-by-step ionospheric assimilation based on ground-based/spaceborne observations and its verification. *Remote Sensing*, *11*(10), 1172. https://doi.org/10.3390/rs11101172

Ge, S., Li, H., Meng, L., Wang, M., Xu, T., Ullah, S., Rauf, A. & Hannachid, A. (2020). On the radar frequency dependence of polar mesosphere summer echoes. *Earth and Planetary Physics*, *4*(6), 1–8. https://doi.org/10.26464/epp2020061

Ge, S., Li, H., Xu, T., Zhu, M., Wang, M., Meng, L., Ullah, S. & Rauf, A. (2019). Characteristics of the layered polar mesosphere summer echoes occurrence ratio observed by EISCAT VHF 224 MHz radar. *Annales Geophysicae*, *37*(3), 417–427. https://doi.org/10.5194/angeo-37-417-2019

Haerendel, G. (2019). Expanding auroral loops. *Journal of Geophysical Research: Space Physics*, *124*(11), 8629–8636. https://doi.org/10.1029/2019ja026983

Han, D.-S., Xu, T., Jin, Y., Oksavik, K., Chen, X.-C., Liu, J.-J., Zhang, Q., Baddeley, L. & Herlingshaw, K. (2019). Observational evidence for throat aurora being associated with magnetopause reconnection. *Geophysical Research Letters*, *46*(13), 7113–7120. https://doi.org/10.1029/2019gl083593

Hosokawa, K., Miyoshi, Y., Ozaki, M., Oyama, S.-I., Ogawa, Y., Kurita, S., Kasahara, Y., Kasaba, Y., Yagitani, S., Matsuda, S., Tsuchiya, F., Kumamoto, A., Kataoka, R., Shiokawa, K., Raita, T., Turunen, E., Takashima, T., Shinohara, I. & Fujii, R. (2020). Multiple time-scale beats in aurora: Precise orchestration via magnetospheric chorus waves. *Scientific Reports*, *10*(1), 3380. https://doi.org/10.1038/s41598-020-59642-8

Hosokawa, K., Kullen, A., Milan, S., Reidy, J., Zou, Y., Frey, H. U., Maggiolo, R. & Fear, R. (2020). Aurora in the polar cap: A review. *Space Science Reviews*, *216*(1), 15. https://doi.org/10.1007/s11214-020-0637-3

Jenner, L. A., Wood, A. G., Dorrian, G. D., Oksavik, K., Yeoman, T. K., Fogg, A. R. & Coster, A. J. (2020). Plasma density gradients at the edge of polar ionospheric holes: The absence of phase scintillation. *Annales Geophysicae*, *38*(2), 575–590. https://doi.org/10.5194/angeo-38-575-2020

Ji, E.-Y., Jee, G. & Lee, C. (2019). Characteristics of the occurrence of ion upflow in association with ion/electron heating in the polar ionosphere. *Journal of Geophysical Research: Space Physics*, *124*(7), 6226–6236. https://doi.org/10.1029/2019ja026799

Jin, Y., Moen, J. I., Spicher, A., Oksavik, K., Miloch, W. J., Clausen, L. B. N., Pożoga, M. & Saito, Y. (2019). Simultaneous rocket and scintillation observations of plasma irregularities associated with a reversed flow event in the cusp ionosphere. *Journal of Geophysical Research: Space Physics*, *124*(8), 7098–7111. https://doi.org/10.1029/2019ja026942

Jin, Y., Xing, Z., Zhang, Q., Wang, Y. & Ma, Y. (2019). Polar cap patches observed by the EISCAT Svalbard radar: A statistical study of its dependence on the solar wind and IMF conditions. *Journal of Atmospheric and Solar-Terrestrial Physics*, *192*, 104768. https://doi.org/10.1016/j.jastp.2018.01.011

Karlsson, T., Andersson, L., Gillies, D. M., Lynch, K., Marghitu, O., Partamies, N., Sivadas, N. & Wu, J. (2020). Quiet, discrete auroral arcs—observations. *Space Science Reviews*, *216*(1), 16. https://doi.org/10.1007/s11214-020-0641-7

Kastinen, D., Tveito, T., Vierinen, J. & Granvik, M. (2020). Radar observability of near-Earth objects using EISCAT 3D. *Annales Geophysicae*, *38*(4), 861–879. https://doi.org/10.5194/angeo-38-861-2020

Kawamura, Y., Hosokawa, K., Nozawa, S., Ogawa, Y., Kawabata, T., Oyama, S.-I., Miyoshi, Y., Kurita, S. & Fujii, R. (2020). Estimation of the emission altitude of pulsating aurora using the five-wavelength photometer. *Earth, Planets and Space*, *72*(1), 96. https://doi.org/10.1186/s40623-020-01229-8

Kim, E., Jee, G., Ji, E.-Y., Kim, Y. H., Lee, C., Kwak, Y.-S. & Shim, J.-S. (2020). Climatology of polar ionospheric density profile in comparison with mid-latitude ionosphere from long-term observations of incoherent scatter radars: A review. *Journal of Atmospheric and Solar-Terrestrial Physics*, *211*, 105449. https://doi.org/10.1016/j.jastp.2020.105449

Kodikara, T., Carter, B., Norman, R. & Zhang, K. (2019). Density-temperature synchrony in the hydrostatic thermosphere. *Journal of Geophysical Research: Space Physics*, *124*(1), 674–699. https://doi.org/10.1029/2018ja025973

Kozlovsky, A., Shalimov, S., Oyama, S., Hosokawa, K., Lester, M., Ogawa, Y. & Hall, C. (2019). Ground echoes observed by the meteor radar and high-speed auroral observations in the substorm growth phase. *Journal of Geophysical Research: Space Physics*, *124*(11), 9278–9292. https://doi.org/10.1029/2019ja026829

Kvammen, A., Gustavsson, B., Sergienko, T., Brändström, U., Rietveld, M., Rexer, T. & Vierinen, J. (2019). The 3-D distribution of artificial aurora induced by HF radio waves in the ionosphere. *Journal of Geophysical Research: Space Physics*, *124*(4), 2992–3006. https://doi.org/10.1029/2018ja025988

Larchenko, A. V., Lebed', O. M., Blagoveshchenskaya, N. F., Pilgaev, S. V., Beketova, E. B. & Fedorenko, Y. V. (2019). Relationship between the polar electrojet dynamics and the amplitude of ELF/VLF signal from the ionospheric source in the modulated ionospheric heating experiment. *Radiophysics and Quantum Electronics*, *62*(6), 385–394. https://doi.org/10.1007/s11141-019-09985-8

Lehtinen, M., Damtie, B. & Orispää, M. (2019). Optimal true time delay filter with application to FPGA firmware-based phased array radar signal processing. *Radio Science*, *54*(9), 810–821. https://doi.org/10.1029/2019rs006821

Lessard, M. R., Fritz, B., Sadler, B., Cohen, I., Kenward, D., Godbole, N., Clemmons, J. H., Hecht, J. H., Lynch, K. A., Harrington, M., Roberts, T. M., Hysell, D., Crowley, G., Sigernes, F., Syrjäsuo, M., Ellingson, P., Partamies, N., Moen, J., Clausen, L., … Yeoman, T. (2020). Overview of the rocket experiment for neutral upwelling sounding rocket 2 (RENU2). *Geophysical Research Letters*, *47*(21), e2018GL081885. https://doi.org/10.1029/2018gl081885

Leyser, T. B., Gustavsson, B., Rexer, T. & Rietveld, M. T. (2020). Electron heating by HF pumping of high-latitude ionospheric F-region plasma near magnetic zenith. *Annales Geophysicae*, *38*(2), 297–307. https://doi.org/10.5194/angeo-38-297-2020

Lu, H., Yang, J., Li, Q., Hao, S., Guo, F., Wu, J., Chen, J., Ma, G. & Xu, T. (2021). ELF/VLF communication experiment by modulated heating of ionospheric auroral electrojet at EISCAT. *IEEE Transactions on Antennas and Propagation*, *69*(4), 2267–2273. https://doi.org/10.1109/tap.2020.3026872

Luque, L. (2020). *Multi-instrument investigation of spectral width in the polar ionosphere* (Master Thesis). Norwegian University of Science and Technology. http://kho.unis.no/doc/Luque_thesis.pdf

Lv, L., Wu, Z., Li, Q., Hao, S., Ma, G., Yang, J., Ding, J. & Wu, J. (2019). Features of downshifted maximum spectra during a dual-pump ionospheric heating experiment. *Advances in Space Research*, *64*(5), 1078–1084. https://doi.org/10.1016/j.asr.2019.06.009

Ma, G., Guo, L., Li, Q., Yang, J., Lv, L., Chen, J., Xu, T., Hao, S. & Wu, J. (2019). Downshifted peak features of stimulated electromagnetic emissions during a two-pump wave heating experiment. *Advances in Space Research*, *64*(7), 1358–1364. https://doi.org/10.1016/j.asr.2019.06.037

Ma, G., Guo, L., Yang, J., Lv, L., Chen, J., Xu, T., Hao, S. & Wu, J. (2019). Effects of variations of geomagnetic field on VLF waves induced by beating of two HF waves. *Advances in Space Research*, *63*(7), 2126–2131. https://doi.org/10.1016/j.asr.2018.12.031

Mahmoudian, A., Senior, A., Kosch, M., Scales, W., Rietveld, M., Isham, B., Shi, X. & Ruohoniemi, M. (2019). Investigation of incoherent scatter radar spectra features with stimulated electromagnetic emissions at EISCAT. *Advances in Space Research*, *64*(1), 159–170. https://doi.org/10.1016/j.asr.2019.03.028

Mahmoudian, A., Yeoman, T., Senior, A., Kosch, M. J., Scales, W., Shi, X., Ruohoniemi, M. & Rietveld, M. (2020). Multi-frequency SuperDARN radar observations of the modulated ionosphere by high-power radio-waves at EISCAT. *Advances in Space Research*, *65*(12), 2791–2799. https://doi.org/10.1016/j.asr.2020.03.020

Mahmoudian, A., Kosch, M. J., Vierinen, J. & Rietveld, M. T. (2020). A new technique for investigating dust charging in the PMSE source region. *Geophysical Research Letters*, *47*(19), e2020GL089639. https://doi.org/10.1029/2020gl089639

Mann, I., Gunnarsdottir, T., Häggström, I., Eren, S., Tjulin, A., Myrvang, M., Rietveld, M., Dalin, P., Jozwicki, D. & Trollvik, H. (2019). Radar studies of ionospheric dusty plasma phenomena. *Contributions to Plasma Physics*, *59*(6), e201900005. https://doi.org/10.1002/ctpp.201900005

Nishimura, Y., Lessard, M. R., Katoh, Y., Miyoshi, Y., Grono, E., Partamies, N., Sivadas, N., Hosokawa, K., Fukizawa, M., Samara, M., Michell, R. G., Kataoka, R., Sakanoi, T., Whiter, D. K., Oyama, S.-i., Ogawa, Y. & Kurita, S. (2020). Diffuse and pulsating aurora. *Space Science Reviews*, *216*(1), 4. https://doi.org/10.1007/s11214-019-0629-3

Ogawa, Y., Seki, K., Keika, K. & Ebihara, Y. (2019). Characteristics of CME- and CIR-driven ion upflows in the polar ionosphere. *Journal of Geophysical Research: Space Physics*, *124*(5), 3637–3649. https://doi.org/10.1029/2018ja025870

Ogawa, Y., Tanaka, Y., Kadokura, A., Hosokawa, K., Ebihara, Y., Motoba, T., Gustavsson, B., Brändström, U., Sato, Y., Oyama, S., Ozaki, M., Raita, T., Sigernes, F., Nozawa, S., Shiokawa, K., Kosch, M., Kauristie, K., Hall, C., Suzuki, S., … Fujii, R. (2020). Development of low-cost multi-wavelength imager system for studies of aurora and airglow. *Polar Science*, *23*, 100501. https://doi.org/10.1016/j.polar.2019.100501

Oyama, S., Shinbori, A., Ogawa, Y., Kellinsalmi, M., Raita, T., Aikio, A., Vanhamäki, H., Shiokawa, K., Virtanen, I., Cai, L., Workayehu, A. B., Pedersen, M., Kauristie, K., Tsuda, T. T., Kozelov, B., Demekhov, A., Yahnin, A., Tsuchiya, F., Kumamoto, A., … Lester, M. (2020). An ephemeral red arc appeared at 68° MLat at a pseudo breakup during geomagnetically quiet conditions. *Journal of Geophysical Research: Space Physics*, *125*(10), e2020JA028468. https://doi.org/10.1029/2020ja028468

Panasenko, S. V., Otsuka, Y., van de Kamp, M., Chernogor, L. F., Shinbori, A., Tsugawa, T. & Nishioka, M. (2019). Observation and characterization of traveling ionospheric disturbances induced by solar eclipse of 20 March 2015 using incoherent scatter radars and GPS networks. *Journal of Atmospheric and Solar-Terrestrial Physics*, *191*, 105051. https://doi.org/10.1016/j.jastp.2019.05.015

Price, D. J., Whiter, D. K., Chadney, J. M. & Lanchester, B. S. (2019). High-resolution optical observations of neutral heating associated with the electrodynamics of an auroral arc. *Journal of Geophysical Research: Space Physics*, *124*(11), 9577–9591. https://doi.org/10.1029/2019ja027345

Rauf, A. (2019). *Effects of energetic particle precipitation on polar mesosphere summer echoes* (PhD Thesis). University of Electronic Science and Technology of China.

Rauf, A., Hailong, L., Ullah, S., Maoyan, W. & Lin, M. (2019). Investigation of PMSE echoes characteristics using the discontinuous EISCAT UHF observation and its relation with space environment. *Advances in Polar Science*, *30*(2), 132–138. https://doi.org/10.13679/j.advps.2018.0041

Rauf, A., Li, H., Ullah, S., Meng, L., Wang, B. & Wang, M. (2019). Investigation of PMSE dependence on high energy particle precipitation during their simultaneous occurrence. *Advances in Space Research*, *63*(1), 309–316. https://doi.org/10.1016/j.asr.2018.09.007

Rietveld, M. T. & Senior, A. (2020). Ducting of incoherent scatter radar waves by field-aligned irregularities. *Annales Geophysicae*, *38*(5), 1101–1113. https://doi.org/10.5194/angeo-38-1101-2020

Rogov, D., Blagoveshchenskaya, N. & Yeoman, T. (2019). Features of artificial ionospheric irregularities induced by powerful HF radio waves from bi-static scatter measurements. *2019 Radiation and Scattering of Electromagnetic Waves (RSEMW)*. https://doi.org/10.1109/rsemw.2019.8792727

Safargaleev, V. V., Kozlovsky, A. E. & Mitrofanov, V. M. (2020). Polar substorm on 7 December 2015: Preonset phenomena and features of auroral breakup. *Annales Geophysicae*, *38*(4), 901–918. https://doi.org/10.5194/angeo-38-901-2020

Sharma, P., Dalin, P. & Mann, I. (2019). Towards a framework for noctilucent cloud analysis. *Remote Sensing*, *11*(23), 2743. https://doi.org/10.3390/rs11232743

Spicher, A., Deshpande, K., Jin, Y., Oksavik, K., Zettergren, M. D., Clausen, L. B. N., Moen, J. I., Hairston, M. R. & Baddeley, L. (2020). On the production of ionospheric irregularities via Kelvin-Helmholtz instability associated with cusp flow channels. *Journal of Geophysical Research: Space Physics*, *125*(6), e2019JA027734. https://doi.org/10.1029/2019ja027734

Stocker, M., Darroch, L., Krahl, R., Habermann, T., Devaraju, A., Schwardmann, U., D'Onofrio, C. & Häggström, I. (2020). Persistent identification of instruments. *Data Science Journal*, *19*(1), 18. https://doi.org/10.5334/dsj-2020-018

Taguchi, S., Hosokawa, K. & Ogawa, Y. (2019). Plasma flow in the north-south aligned discrete aurora equatorward of the cusp. *Journal of Geophysical Research: Space Physics*, *124*(12), 10778–10793. https://doi.org/10.1029/2019ja026895

Takahashi, T., Virtanen, I. I., Hosokawa, K., Ogawa, Y., Aikio, A., Miyaoka, H. & Kero, A. (2019). Polarization electric field inside auroral patches: Simultaneous experiment of EISCAT radars and KAIRA. *Journal of Geophysical Research: Space Physics*, *124*(5), 3543–3557. https://doi.org/10.1029/2018ja026254

Tereshchenko, E. D., Cherniakov, S. M., Yurik, R. Y., Rietveld, M. T. & Häggström, I. (2020). Total electron content measurements in the ionosphere disturbed by high-power high-frequency waves by the methods of incoherent scattering of radio waves and radio sounding by glonass satellite signal. *Radiophysics and Quantum Electronics*, *62*(10), 667–676. https://doi.org/10.1007/s11141-020-10012-4

Tesema, F., Partamies, N., Tyssøy, H. N. & McKay, D. (2020). Observations of precipitation energies during different types of pulsating aurora. *Annales Geophysicae*, *38*(6), 1191–1202. https://doi.org/10.5194/angeo-38-1191-2020

Themens, D. R., Jayachandran, P., McCaffrey, A. M., Reid, B. & Varney, R. H. (2019). A bottomside parameterization for the empirical Canadian high Arctic ionospheric model. *Radio Science*, *54*(5), 397–414. https://doi.org/10.1029/2018rs006748

Tsuda, T. T., Li, C., Hamada, S., Hosokawa, K., Oyama, S.-i., Nozawa, S., Kawabata, T., Mizuno, A., Kurihara, J., Nishiyama, T. & Kosch, M. J. (2020). OI 630.0-nm and $N_2$ 1PG emissions in pulsating aurora events observed by an optical spectrograph at Tromsø, Norway. *Journal of Geophysical Research: Space Physics*, *125*(12), e2020JA028250. https://doi.org/10.1029/2020ja028250

Ullah, S. (2019). *The effect of artificial electron heating on polar mesosphere echoes* (PhD Thesis). University of Electronic Science and Technology of China.

Ullah, S., Li, H.-L., Rauf, A., Fu, L.-Y., Wang, M.-Y. & Meng, L. (2020). Numerical analysis of artificial electron heating effects on polar mesospheric winter echoes. *Journal of Electronic Science and Technology*, *18*(3), 287–295. https://doi.org/10.11989/JEST.1674-862X.80521012

Ullah, S., Li, H., Rauf, A., Meng, L., Wang, B. & Wang, M. (2019). Statistical study of PMSE response to HF heating in two altitude regions. *Earth, Planets and Space*, *71*(1), 22. https://doi.org/10.1186/s40623-019-1007-9

Wang, X., Zhou, C., Xu, T., Honary, F., Rietveld, M. & Frolov, V. (2019). Stimulated electromagnetic emissions spectrum observed during an X-mode heating experiment at the European incoherent scatter scientific association. *Earth and Planetary Physics*, *3*(5), 391–399. https://doi.org/10.26464/epp2019042

Wharton, S. J., Wright, D. M., Yeoman, T. K. & Reimer, A. S. (2019). Identifying ULF wave eigenfrequencies in SuperDARN backscatter using a Lomb-Scargle cross-phase analysis. *Journal of Geophysical Research: Space Physics*, *124*(2), 996–1012. https://doi.org/10.1029/2018ja025859

Wu, J., Wu, J., Rietveld, M. T., Haggstrom, I., Xu, Z., Zhang, Y., Xu, T. & Zhao, H. (2019). The intensities of high frequency-enhanced plasma and ion lines during ionospheric heating. *Journal of Geophysical Research: Space Physics*, *124*(1), 603–615. https://doi.org/10.1029/2018ja025918

Wu, Q., Knipp, D., Liu, J., Wang, W., Häggström, I., Jee, G., Kwak, Y.-S. & Erickson, P. J. (2019). What do the new 2018 HIWIND thermospheric wind observations tell us about high-latitude ion-neutral coupling during daytime? *Journal of Geophysical Research: Space Physics*, *124*(7), 6173–6181. https://doi.org/10.1029/2019ja026776

Xu, H., Shiokawa, K., Oyama, S.-i. & Nozawa, S. (2019). High-latitude thermospheric wind study using a Fabry-Perot interferometer at Tromsø in Norway: Averages and variations during quiet times. *Earth, Planets and Space*, *71*(1), 110. https://doi.org/10.1186/s40623-019-1093-8

Xu, H., Shiokawa, K., Oyama, S.-i. & Otsuka, Y. (2019). Thermospheric wind variations observed by a Fabry-Perot interferometer at Tromsø, Norway, at substorm onsets. *Earth, Planets and Space*, *71*(1), 93. https://doi.org/10.1186/s40623-019-1072-0

Xu, T., Rietveld, M., Wu, J., Ma, G., Hu, Y., Wu, J. & Li, Q. (2019). Polarization analysis of ELF/VLF waves generated by beating of two HF waves in the polar ionosphere. *Journal of Atmospheric and Solar-Terrestrial Physics*, *196*, 105133. https://doi.org/10.1016/j.jastp.2019.105133

Yamauchi, M., Johnsen, M. G., Enell, C.-F., Tjulin, A., Willer, A. & Sormakov, D. A. (2020). High-latitude crochet: Solar-flare-induced magnetic disturbance independent from low-latitude crochet. *Annales Geophysicae*, *38*(6), 1159–1170. https://doi.org/10.5194/angeo-38-1159-2020

Yang, J., Li, Q., Lu, H., Che, H., Hao, S., Guo, F., Wu, J., Lyu, L., Chen, J., Ma, G. & Xu, T. (2020). CSES observations of ELF wave radiation excited by the EISCAT heater. *Physics of Plasmas*, *27*(12), 122903. https://doi.org/10.1063/5.0022474

Yang, J., Wang, J., Li, Q., Wu, J., Che, H., Ma, G. & Hao, S. (2019). Experimental comparisons between AM and BW modulation heating excitation of ELF/VLF waves at EISCAT. *Physics of Plasmas*, *26*(8), 082901. https://doi.org/10.1063/1.5095537

# EISCAT Operations 2019 and 2020

The EISCAT radars operate in two basic modes, using approximately half the available observing time for each. In the Special Programme mode, users conduct individual experiments dedicated to specific experiments and objectives. The resulting data are reserved for the exclusive use of the experimenters for one year from the date of collection. Special programmes often make use of the well developed pulse schemes and observing modes of the Common Programme. EISCAT Common Programmes are conducted for the benefit of the entire user community and the resulting data are immediately available to all.

The UHF and VHF radars are often operated simultaneously during the Common Programme experiments. Such observations offer comprehensive data sets for atmospheric, ionospheric, and magnetospheric studies.

Common Programme One, CP-1, uses a fixed transmitting antenna, pointing along the geomagnetic field direction. The three-dimensional velocity and anisotropy in other parameters are measured by means of the VHF receiving stations at Kiruna and Sodankylä. CP-1 is capable of providing results with very good time resolution and is suitable for the study of substorm phenomena, particularly auroral processes where conditions might change rapidly. Continuous electric field measurements are derived from the tri-static F-region data. On longer time scales, CP-1 measurements support studies of diurnal changes, such as atmospheric tides, as well as seasonal and solar-cycle variations.

Common Programme Two, CP-2, is designed to make measurements from a small, rapid transmitter antenna scan. One aim is to identify wave-like phenomena with length and time scales comparable with, or larger than, the scan (a few tens of kilometers and about ten minutes). The first three positions form a triangle with vertical, south, and south-east positions, while the fourth is aligned with the geomagnetic field.

Common Programme Three, CP-3, covers a 10° latitudinal range in the F-region with a 17-position scan up to 74°N in a 30 min cycle. The observations are made in a plane defined by the magnetic meridian through Tromsø. The principal aim of CP-3 is the mapping of ionospheric and electrodynamic parameters over a broad latitude range.

Common Programme Four, CP-4, covers geographic latitudes up to almost 80°N (77°N invariant latitude) using a low elevation, split-beam configuration. CP-4 is particularly suitable for studies of high latitude plasma convection and polar cap phenomena. However, with the present one-beam configuration of the VHF radar, CP-4 is run with either both UHF and VHF radars or with UHF only in a two position scan.

Common Programme Six, CP-6, is designed for low altitude studies, providing spectral measurements at mesospheric heights. Velocity and electron density are derived from the measurements and the spectra contain information on the aeronomy of the mesosphere. Vertical antenna pointing is used.

Common Programme Seven, CP-7, probes high altitudes and is particularly aimed at polar wind studies. The present version, with only one of the VHF klystrons running, is designed to cover altitudes up to 1500 km vertically above Ramfjordmoen.

Equivalent Common Programme modes are available for the EISCAT Svalbard Radar: CP-1 is directed along the geomagnetic field (81.6° inclination). CP-2 uses a four position scan. CP-3 is a 15 position elevation scan with southerly beam swinging positions. CP-4 combines observations in the F-region viewing area with field-aligned and vertical measurements. CP-6 is similar to the mainland radar CP-6. CP-7 is similar to the mainland radar CP-7.

The tables on the next four pages summarise the accounted hours on the various facilities for each month and for each Common Programme mode (CP) or Associate (SP) for the years 2019 and 2020.

2019

## KST COMMON PROGRAMMES

| 2019 | Jan | Feb | Mar | Apr | May | Jun | Jul | Aug | Sept | Oct | Nov | Dec | Total | % | Target% |
|---|---|---|---|---|---|---|---|---|---|---|---|---|---|---|---|
| **CP1** | | | | | 46.5 | | | 6 | | | 0.5 | 15 | 68 | 11 | 16 |
| **CP2** | 140.5 | 110 | | | | | | | | | | | 250.5 | 42 | 16 |
| **CP3** | | | 73 | | | | | | | | | | 73 | 12 | 12 |
| **CP4** | | | | | | | | 7.5 | 161.5 | | | 0.5 | 169.5 | 28 | 10 |
| **CP6** | | | | | | 40.5 | 1.5 | | | | | | 42 | 7 | 20 |
| **CP7** | | | | | | | | | | | 0.5 | | 0.5 | 0 | 18 |
| **UP** | | | | | | | | | | | | | 0 | 0 | |
| **Total** | 140.5 | 110 | 73 | 0 | 46.5 | 40.5 | 1.5 | 13.5 | 161.5 | 0 | 1 | 15.5 | **603.5** | 100 | |
| % | 23 | 18 | 12 | 0 | 8 | 7 | 0 | 2 | 27 | 0 | 0 | 3 | 100 | | |

## KST SPECIAL PROGRAMMES

| 2019 | Jan | Feb | Mar | Apr | May | Jun | Jul | Aug | Sept | Oct | Nov | Dec | Total | Incl AA | Move | Target |
|---|---|---|---|---|---|---|---|---|---|---|---|---|---|---|---|---|
| **CN** | | | | | | | | | | | 75.5 | | 75.5 | 84 | | 87 |
| **FI** | 13 | | | | | 17 | 15 | | | | 29.5 | | 74.5 | 82 | | 80 |
| **NI** | 39 | 10.5 | 16 | | | | | | 5 | 2.5 | | 21.5 | 94.5 | 106 | -6 | 112 |
| **NO** | 19.5 | | 7.5 | 18.5 | | 12 | 19.5 | 22 | | 2.5 | 3.5 | 14 | 119 | 133 | | 146 |
| **SW** | | | 18.5 | 14.5 | | 12 | | 22 | | 45 | 12 | 2 | 126 | 148 | | 233 |
| **UK** | 8 | | | | | | 34.5 | | | 2.5 | 20 | 26 | 91 | 121 | | 312 |
| **AA** | | | | | | | | | 33 | 24 | 22 | 15 | 94 | | | |
| **Total** | 79.5 | 10.5 | 42 | 33 | 0 | 41 | 69 | 44 | 38 | 76.5 | 162.5 | 78.5 | **674.5** | **675** | **-6** | **976** |
| **%** | 12 | 2 | 6 | 5 | 0 | 6 | 10 | 7 | 6 | 11 | 24 | 12 | 100 | | | |

| | EI | CN | FI | NI | NO | SW | UK | |
|---|---|---|---|---|---|---|---|---|
| **Target** | | 8.87 | 8.21 | 12.13 | 14.92 | 23.91 | 31.96 | % |

## KST OTHER PROGRAMMES

| 2019 | Jan | Feb | Mar | Apr | May | Jun | Jul | Aug | Sept | Oct | Nov | Dec | Total | Target |
|---|---|---|---|---|---|---|---|---|---|---|---|---|---|---|
| **PP** | | | | | | | | | | | 4.5 | 5 | 9.5 | 40 |
| **EI** | | | | | | | | | | | | | 0 | 28 |
| **RU** | | | | | | | | | | 24 | | | 24 | 0 |
| **FR** | | | | | | | | | | | | | 0 | 4 |
| **UA** | | | | | | | | | | | | | 0 | 7 |
| **KR** | | | | | | | | | | | | | 0 | 0 |
| **TB** | | | | | | | | | | | | | 0 | 0 |
| **Total** | 0 | 0 | 0 | 0 | 0 | 0 | 0 | 0 | 0 | 24 | 4.5 | 5 | **33.5** | **164** |

## KST TOTALS

| 2019 | Jan | Feb | Mar | Apr | May | Jun | Jul | Aug | Sept | Oct | Nov | Dec | Total | Target |
|---|---|---|---|---|---|---|---|---|---|---|---|---|---|---|
| **CP** | 140.5 | 110 | 73 | 0 | 46.5 | 40.5 | 1.5 | 13.5 | 161.5 | 0 | 1 | 15.5 | 603.5 | 504 |
| **SP** | 79.5 | 10.5 | 42 | 33 | 0 | 41 | 69 | 44 | 38 | 76.5 | 162.5 | 78.5 | 674.5 | 982 |
| **OP** | 0 | 0 | 0 | 0 | 0 | 0 | 0 | 0 | 0 | 24 | 4.5 | 5 | 33.5 | 164 |
| **Total** | 220 | 120.5 | 115 | 33 | 46.5 | 81.5 | 70.5 | 57.5 | 199.5 | 100.5 | 168 | 99 | **1311.5** | **1650** |

## USAGE BREAKDOWN

| 2019 | Jan | Feb | Mar | Apr | May | Jun | Jul | Aug | Sept | Oct | Nov | Dec | Total | Target |
|---|---|---|---|---|---|---|---|---|---|---|---|---|---|---|
| **UHF** | 162.5 | 120 | 104.5 | 33 | 46.5 | 31 | | 6 | 35 | 57.5 | 104 | 49.5 | 749.5 | 687 |
| **VHF** | 57 | | 9 | | | 37 | 42 | 40 | 119 | 13 | 15 | 46 | 378 | 687 |
| **ESR** | 129 | 143.5 | 94 | 0 | 55 | 34.5 | 0 | 14 | 119 | 10 | 59 | 73 | 731 | 935 |
| **Heating** | | | | | | | 22 | | | 29.5 | 44 | 0.5 | 96 | 156 |
| **Total Radar** | 348.5 | 263.5 | 207.5 | 33 | 101.5 | 102.5 | 64 | 60 | 273 | 110 | 222 | 169 | 1858.5 | 2465 |
| **Low Power V** | | | | | | | | | | | | | 0 | |
| **Passive KST** | | | 8.5 | | | 66.5 | | 58 | 226.5 | | 25.5 | 18 | 403 | 600 |
| **Passive ESR** | | | | | | | | | | | | | 0 | |

## 2019

### ESR COMMON PROGRAMMES

| 2019 | Jan | Feb | Mar | Apr | May | Jun | Jul | Aug | Sept | Oct | Nov | Dec | Total | % | Target% |
|---|---|---|---|---|---|---|---|---|---|---|---|---|---|---|---|
| **CP1** | 62 | 45.5 | 70 | | 47 | 1 | | | | 6 | | | 231.5 | 50 | 54 |
| **CP2** | 21 | 63 | | | | | | | | | | | 84 | 18 | 16 |
| **CP3** | | | | | | | | 2 | 119 | | | | 121 | 26 | 12 |
| **CP4** | | | | | | | | 4 | | | | | 4 | 1 | 10 |
| **CP6** | | | | | | 26 | | | | | | | 26 | 6 | |
| **CP7** | | | | | | | | | | | | | 0 | 0 | |
| **UP** | | | | | | | | | | | | | 0 | 0 | |
| **Total** | 83 | 108.5 | 70 | 0 | 47 | 27 | 0 | 6 | 119 | 6 | 0 | 0 | **466.5** | 100 | |
| % | 18 | 23 | 15 | 0 | 10 | 6 | 0 | 1 | 26 | 1 | 0 | 0 | 100 | | |

### ESR SPECIAL PROGRAMMES

| 2019 | Jan | Feb | Mar | Apr | May | Jun | Jul | Aug | Sept | Oct | Nov | Dec | Total | Incl AA | Move | Target |
|---|---|---|---|---|---|---|---|---|---|---|---|---|---|---|---|---|
| **CN** | | | | | | | | | | | | | 0 | 0 | 0 | 37 |
| **FI** | | | | | | 7.5 | | | | | | | 7.5 | 8 | 0 | 34 |
| **NI** | | | 12 | | | | | | | | 3.5 | 23.5 | 39 | 39 | 6 | 57 |
| **NO** | 1 | 11 | 4 | | | | | | | | 10 | 8.5 | 34.5 | 35 | 0 | 63 |
| **SW** | 25 | 24 | | | | | | | | | 21.5 | 2 | 72.5 | 73 | 0 | 100 |
| **UK** | 12 | | | | | | | 8 | | 4 | 20.5 | 21.5 | 66 | 66 | 0 | 134 |
| **AA** | | | | | | | | | | | | | 0 | | | |
| **Total** | 38 | 35 | 16 | 0 | 0 | 7.5 | 0 | 8 | 0 | 4 | 55.5 | 55.5 | **219.5** | **220** | **6** | **420** |
| **%** | 17 | 16 | 7 | 0 | 0 | 3 | 0 | 4 | 0 | 2 | 25 | 25 | 100 | | | |

### ESR OTHER PROGRAMMES

| 2019 | Jan | Feb | Mar | Apr | May | Jun | Jul | Aug | Sept | Oct | Nov | Dec | Total | Target |
|---|---|---|---|---|---|---|---|---|---|---|---|---|---|---|
| **PP** | 8 | | 8 | | | | | | | | 3.5 | 5.5 | 25 | 36 |
| **EI** | | | | | 8 | | | | | | | | 8 | 22 |
| **RU** | | | | | | | | | | | | | 0 | 0 |
| **FR** | | | | | | | | | | | | 12 | 12 | 0 |
| **UA** | | | | | | | | | | | | | 0 | 0 |
| **KR** | | | | | | | | | | | | | 0 | 34 |
| **TB** | | | | | | | | | | | | | 0 | 0 |
| **Total** | 8 | 0 | 8 | 0 | 8 | 0 | 0 | 0 | 0 | 0 | 3.5 | 17.5 | **45** | **92** |

### ESR TOTALS

| 2019 | Jan | Feb | Mar | Apr | May | Jun | Jul | Aug | Sept | Oct | Nov | Dec | Total | Target |
|---|---|---|---|---|---|---|---|---|---|---|---|---|---|---|
| **CP** | 83 | 108.5 | 70 | 0 | 47 | 27 | 0 | 6 | 119 | 6 | 0 | 0 | 466.5 | 429 |
| **SP** | 38 | 35 | 16 | 0 | 0 | 7.5 | 0 | 8 | 0 | 4 | 55.5 | 55.5 | 219.5 | 414 |
| **OP** | 8 | 0 | 8 | 0 | 8 | 0 | 0 | 0 | 0 | 0 | 3.5 | 17.5 | 45 | 92 |
| **Total** | 129 | 143.5 | 94 | 0 | 55 | 34.5 | 0 | 14 | 119 | 10 | 59 | 73 | **731** | **935** |

# 2020

### KST COMMON PROGRAMMES

| 2020 | Jan | Feb | Mar | Apr | May | Jun | Jul | Aug | Sept | Oct | Nov | Dec | Total | % | Target% |
|---|---|---|---|---|---|---|---|---|---|---|---|---|---|---|---|
| **CP1** | 0.5 | 119.5 | 0.5 | | | 1 | | | 6 | | 4 | 55 | 186.5 | 37 | 16 |
| **CP2** | | 208.5 | | | | | | | | | | | 208.5 | 41 | 16 |
| **CP3** | | | | | | | | | | | | | 0 | 0 | 12 |
| **CP4** | | | | | | | | | | | | | 0 | 0 | 10 |
| **CP6** | | | | | | 42 | 11 | | | | 3.5 | | 56.5 | 11 | 20 |
| **CP7** | | | | | | | | | 47 | | 1.5 | 2.5 | 51 | 10 | 18 |
| **UP** | | | | | | | | | | | | | 0 | 0 | |
| **Total** | 0.5 | 328 | 0.5 | 0 | 0 | 43 | 11 | 0 | 53 | 0 | 9 | 57.5 | **502.5** | 100 | |
| **%** | 0 | 65 | 0 | 0 | 0 | 9 | 2 | 0 | 11 | 0 | 2 | 11 | 100 | | |

### KST SPECIAL PROGRAMMES

| 2020 | Jan | Feb | Mar | Apr | May | Jun | Jul | Aug | Sept | Oct | Nov | Dec | Total | Incl AA | Move | Target |
|---|---|---|---|---|---|---|---|---|---|---|---|---|---|---|---|---|
| **CN** | | | | | | | | | | | | | 0 | 5 | | 53 |
| **FI** | | 32 | | | | | | | | | 46 | 8 | 86 | 95 | | 86 |
| **NI** | | 10 | | | | | | | | | 16 | 55.5 | 81.5 | 90 | | 85 |
| **NO** | | | | | | | 21.5 | 36 | 22.5 | | | 2 | 82 | 98 | | 159 |
| **SW** | 5 | 43 | 71 | | | | | 25.5 | | 22 | | | 166.5 | 196 | | 286 |
| **UK** | 36 | | | | | | | | 24.5 | | | 24 | 84.5 | 112 | | 269 |
| **AA** | 8 | 11.5 | 20 | | | | | | | 19 | 11.5 | 21 | 91 | | | |
| **Total** | 49 | 96.5 | 91 | 0 | 0 | 0 | 21.5 | 61.5 | 47 | 41 | 73.5 | 110.5 | **591.5** | **596** | **0** | **891** |
| **%** | 8 | 16 | 15 | 0 | 0 | 0 | 4 | 10 | 8 | 7 | 12 | 19 | 100 | | | |

| | EI | CN | FI | NI | NO | SW | UK | |
|---|---|---|---|---|---|---|---|---|
| **Target** | | 5.97 | 9.6 | 9.52 | 17.82 | 32.15 | 30.18 | % |

### KST OTHER PROGRAMMES

| 2020 | Jan | Feb | Mar | Apr | May | Jun | Jul | Aug | Sept | Oct | Nov | Dec | Total | Target |
|---|---|---|---|---|---|---|---|---|---|---|---|---|---|---|
| **PP** | | 24 | | | | | | | | 44.5 | | 4 | 72.5 | 77 |
| **EI** | | | | | | | | | | | | | 0 | 28 |
| **GE** | | | | | | 22.5 | | | | | | | 22.5 | 28 |
| **FR** | | 6 | | | | | | | | | | | 6 | 7 |
| **UA** | | | | | | 16.5 | | | | | | | 16.5 | 5 |
| **KR** | | | | | | | | | | | | | 0 | 0 |
| **US** | | | | | | 7 | | | | | | | 7 | 7 |
| **TB** | | | | | | | | | | | | | 0 | 0 |
| **Total** | 0 | 30 | 0 | 0 | 0 | 46 | 0 | 0 | 0 | 44.5 | 0 | 4 | **124.5** | **152** |

### KST TOTALS

| 2020 | Jan | Feb | Mar | Apr | May | Jun | Jul | Aug | Sept | Oct | Nov | Dec | Total | Target |
|---|---|---|---|---|---|---|---|---|---|---|---|---|---|---|
| **CP** | 0.5 | 328 | 0.5 | 0 | 0 | 43 | 11 | 0 | 53 | 0 | 9 | 57.5 | 502.5 | 504 |
| **SP** | 49 | 96.5 | 91 | 0 | 0 | 0 | 21.5 | 61.5 | 47 | 41 | 73.5 | 110.5 | 591.5 | 891 |
| **OP** | 0 | 30 | 0 | 0 | 0 | 46 | 0 | 0 | 0 | 44.5 | 0 | 4 | 124.5 | 152 |
| **Total** | 49.5 | 454.5 | 91.5 | 0 | 0 | 89 | 32.5 | 61.5 | 100 | 85.5 | 82.5 | 172 | **1218.5** | **1547** |

### USAGE BREAKDOWN

| 2020 | Jan | Feb | Mar | Apr | May | Jun | Jul | Aug | Sept | Oct | Nov | Dec | Total | Target |
|---|---|---|---|---|---|---|---|---|---|---|---|---|---|---|
| **UHF** | 46 | 400.5 | 45.5 | | | 12 | | | 29 | 65 | 39 | 106 | 743 | 696 |
| **VHF** | | 40.5 | 22.5 | | | 30 | 41 | 39.5 | 47 | | 44.5 | 64.5 | 329.5 | 696 |
| **ESR** | 71.5 | 362.5 | 0 | 0 | 0 | 24 | 0 | 0 | 37 | 0 | 40.5 | 164 | 699.5 | 948 |
| **Heating** | | | 23.5 | | | 12.5 | | 7.5 | 24.5 | 20.5 | | 2 | 90.5 | 155 |
| **Total Radar** | 117.5 | 803.5 | 91.5 | 0 | 0 | 78.5 | 41 | 47 | 137.5 | 85.5 | 124 | 336.5 | 1916 | 2495 |
| **Passive KST** | | 66.5 | | | | 60 | 69 | 72.5 | | | | | 268 | |
| **Passive ESR** | | | | | | | | | | | | | 0 | |

## 2020

### ESR COMMON PROGRAMMES

| **2020** | **Jan** | **Feb** | **Mar** | **Apr** | **May** | **Jun** | **Jul** | **Aug** | **Sept** | **Oct** | **Nov** | **Dec** | **Total** | **%** | **Target%** |
|---|---|---|---|---|---|---|---|---|---|---|---|---|---|---|---|
| **CP1** | | 246.5 | | | | | | | | | | 60 | 306.5 | 69 | 54 |
| **CP2** | | | | | | | | | | | | | 0 | 0 | 16 |
| **CP3** | | | | | | | | | | | | | 0 | 0 | 12 |
| **CP4** | | 74.5 | | | | | | | | | | | 74.5 | 17 | 10 |
| **CP6** | | | | | | 24 | | | | | | | 24 | 5 | |
| **CP7** | | | | | | | | | 37 | | | 1 | 38 | 9 | |
| **UP** | | | | | | | | | | | | | 0 | 0 | |
| **Total** | 0 | 321 | 0 | 0 | 0 | 24 | 0 | 0 | 37 | 0 | 0 | 61 | **443** | 100 | |
| % | 0 | 72 | 0 | 0 | 0 | 5 | 0 | 0 | 8 | 0 | 0 | 14 | 100 | | |

### ESR SPECIAL PROGRAMMES

| **2020** | **Jan** | **Feb** | **Mar** | **Apr** | **May** | **Jun** | **Jul** | **Aug** | **Sept** | **Oct** | **Nov** | **Dec** | **Total** | **Incl AA** | **Move** | **Target** |
|---|---|---|---|---|---|---|---|---|---|---|---|---|---|---|---|---|
| **CN** | | | | | | | | | | | | | 0 | 0 | 0 | 30 |
| **FI** | | 12 | | | | | | | | | 32.5 | | 44.5 | 45 | 0 | 48 |
| **NI** | 8 | | | | | | | | | | 8 | 34 | 50 | 50 | 0 | 48 |
| **NO** | 12 | 16.5 | | | | | | | | | | | 28.5 | 29 | 0 | 89 |
| **SW** | | 13 | | | | | | | | | | | 13 | 13 | 0 | 160 |
| **UK** | 51.5 | | | | | | | | | | | 69 | 120.5 | 121 | 0 | 151 |
| **AA** | | | | | | | | | | | | | 0 | | | |
| **Total** | 71.5 | 41.5 | 0 | 0 | 0 | 0 | 0 | 0 | 0 | 0 | 40.5 | 103 | **256.5** | **257** | **0** | **499** |
| **%** | 28 | 16 | 0 | 0 | 0 | 0 | 0 | 0 | 0 | 0 | 16 | 40 | 100 | | | |

### ESR OTHER PROGRAMMES

| **2020** | **Jan** | **Feb** | **Mar** | **Apr** | **May** | **Jun** | **Jul** | **Aug** | **Sept** | **Oct** | **Nov** | **Dec** | **Total** | **Target** |
|---|---|---|---|---|---|---|---|---|---|---|---|---|---|---|
| **PP** | | | | | | | | | | | | | 0 | 0 |
| **EI** | | | | | | | | | | | | | 0 | 22 |
| **GE** | | | | | | | | | | | | | 0 | 0 |
| **FR** | | | | | | | | | | | | | 0 | 0 |
| **UA** | | | | | | | | | | | | | 0 | 0 |
| **KR** | | | | | | | | | | | | | 0 | 31 |
| **TB** | | | | | | | | | | | | | 0 | 0 |
| **Total** | 0 | 0 | 0 | 0 | 0 | 0 | 0 | 0 | 0 | 0 | 0 | 0 | **0** | **53** |

### ESR TOTALS

| **2020** | **Jan** | **Feb** | **Mar** | **Apr** | **May** | **Jun** | **Jul** | **Aug** | **Sept** | **Oct** | **Nov** | **Dec** | **Total** | **Target** |
|---|---|---|---|---|---|---|---|---|---|---|---|---|---|---|
| **CP** | 0 | 321 | 0 | 0 | 0 | 24 | 0 | 0 | 37 | 0 | 0 | 61 | 443 | 396 |
| **SP** | 71.5 | 41.5 | 0 | 0 | 0 | 0 | 0 | 0 | 0 | 0 | 40.5 | 103 | 256.5 | 499 |
| **OP** | 0 | 0 | 0 | 0 | 0 | 0 | 0 | 0 | 0 | 0 | 0 | 0 | 0 | 53 |
| **Total** | 71.5 | 362.5 | 0 | 0 | 0 | 24 | 0 | 0 | 37 | 0 | 40.5 | 164 | **699.5** | **948** |

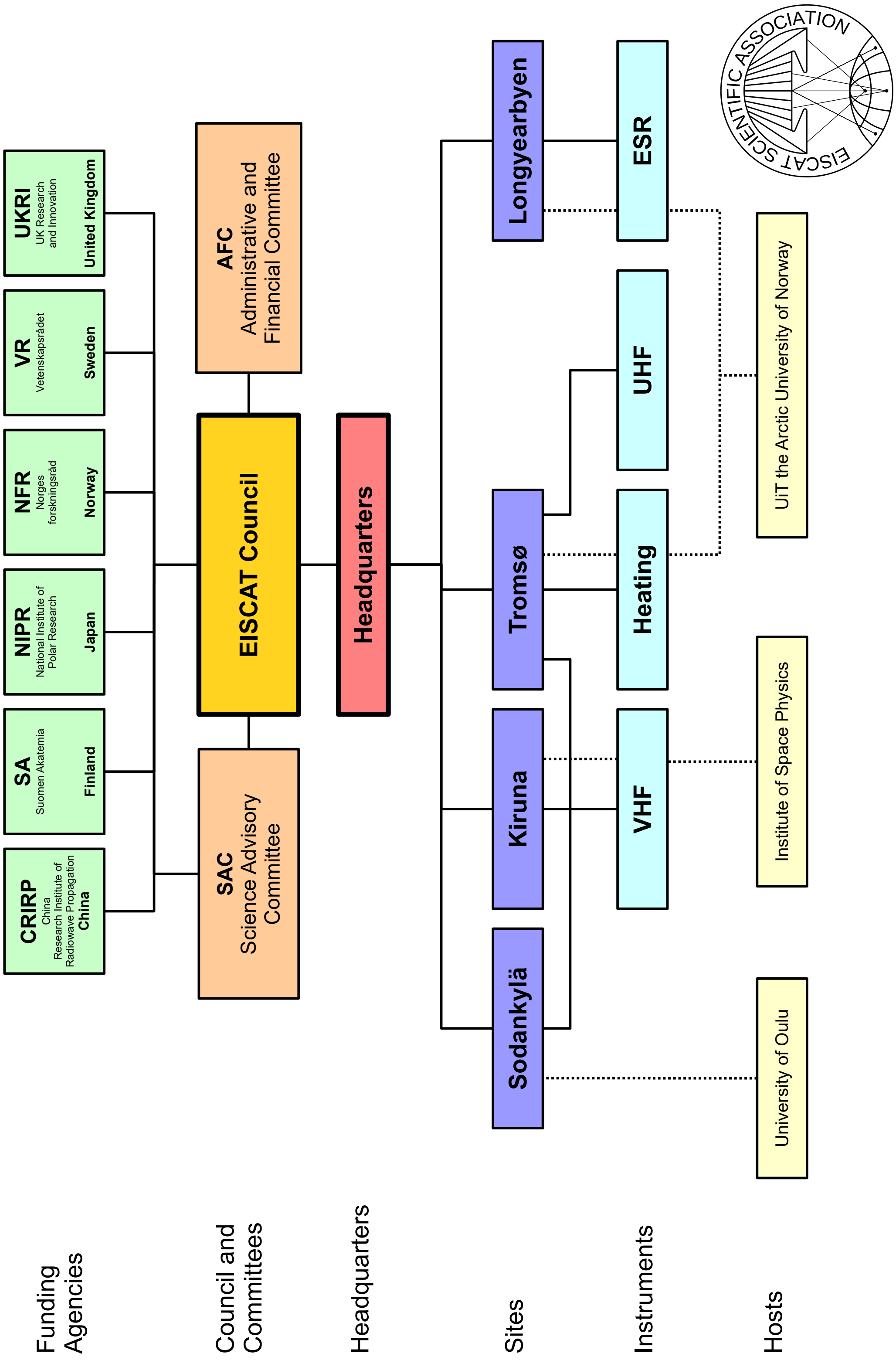

EISCAT organisational diagram, December 2020.

Photo from the Annual Review Meeting, 4–7 November 2019, at Arctic River Lodge in Tärendö, Sweden. From left: Emma Unander, Ingemar Häggström, Henrik Andersson, Johan Svensson, Harri Hellgren, Lennart Lövqvist, Anders Tjulin, Carl-Fredrik Enell, Erlend Danielsen, Juri Katkalov, Craig Heinselman, Jussi Markkanen, Taishi Hashimoto, Erik Varberg, David Rutberg, Mike Rietveld, Simon Brown, Elisabet Goth, Assar Westman, Esa Wikström, Arild Stenberg, Rikard Slapak, Espen Helgesen, Robert Juhlin, Guttorm Mikalsen.

# EISCAT Scientific Association

## December 2020

## Council

The Council consists of a Delegation with a maximum of three persons from each Associate.

| | |
|---|---|
| **Finland** | |
| Prof. A. Aikio | *Vice-Chair* |
| Dr. K. Sulonen | Delegate |
| Dr. J. Virtanen | |
| **Japan** | |
| Prof. H. Miyaoka | Delegate |
| Dr. S. Nozawa | |
| **Norway** | |
| Prof. P. Espy | |
| Prof. I. Mann | *Chair* |
| Prof. K. Ruud | Delegate |
| **P. R. of China** | |
| Dr. Z. Ding | |
| Prof. J. Wu | Delegate |
| **Sweden** | |
| Dr. T. Andersson | Delegate |
| Prof. J. Gumbel | |
| **United Kingdom** | |
| Prof. M. Freeman | Delegate |
| Dr. I. W. McCrea | |

## Scientific Advisory Committee

The EISCAT scientific community organises the Scientific Oversight Committee (SAC), under the guidance of the Council.

| | |
|---|---|
| Prof. L. Baddeley | Norway |
| Dr. J. Berdermann | Germany (affiliated) |
| Dr. S. Buchert | Sweden |
| Prof. J. Chau | External member |
| Prof. A. Coster | External member |
| Dr. G. Jee | S. Korea (affiliated) |
| Dr. A. Kavanagh | *Chairperson*, United Kingdom |
| Dr. Y.-S. Kwak | S. Korea (affiliated) |
| Dr. Y. Ogawa | Japan |
| Dr. F. Pitout | France (affiliated) |
| Dr. T. Ulich | Finland |
| Dr. J. Wu | P. R. of China |
| Dr. A. Zalizovsky | Ukraine |

## Director

Dr. C. Heinselman

## Administrative and Finance Committee

The Administrative and Finance Committee (AFC) advises the EISCAT Council on matters relating to administrative, financial and legal issues.

| | |
|---|---|
| Mr. H. Andersson | Head of Administration |
| Mr. B. Clark | United Kingdom |
| Dr. M. Friberg | *Chairperson*, Sweden |
| Dr, C. Heinselman | Director |
| Prof. H. Miyaoka | Japan |
| Dr. I. Solheim | Norway |
| Ms. M. Vannas | Finland |

## Executives

Senior Management

| | |
|---|---|
| Mr. H. Andersson | Head of Adm., Deputy Dir. |
| Dr. C. Heinselman | Director |

## Site Leaders

Station Managers

| | |
|---|---|
| Mr. E. Helgesen | EISCAT Svalbard Radar |
| Dr. I. Häggström | Kiruna Site (acting) |
| Mr. J. Markkanen | Sodankylä Site |
| Dr. M. Rietveld | Tromsø Radar & Heating |

# Appendix:

# EISCAT Scientific Association Annual Report, 2019

EISCAT Scientific Association
Registered as a Swedish non-profit organisation
Organisation number: 897300-2549

Annual financial report for the year 2019-01-01 – 2019-12-31

The EISCAT Council and the Director for the Association submits herewith the annual report for 2019.

## ADMINISTRATION REPORT

**Ownership, organisation and objective**
The EISCAT Scientific Association was established in 1975 through an agreement between six European organisations. Japan joined in 1996 and the People's Republic of China in 2007.

The EISCAT Associates at 2019-12-31 are: China Research Institute of Radiowave Propagation (People's Republic of China), National Institute of Polar Research (Japan), Norges forskningsråd (Norway), Suomen Akatemia (Finland), UK Research and Innovation (United Kingdom of Great Britain and Northern Ireland) and Vetenskapsrådet (Sweden).

The now running EISCAT Agreement came into force 2017-06-20, with all Associates making long term funding commitments to the Association. The Association has its formal seat in Kiruna, Sweden, and is registered as a non-profit organisation.

The aim of the Association is to make significant progress in the understanding of physical processes in geospace, in the high latitude atmosphere, and in the coupling between the high and low latitudes and altitudes. For this purpose, the Association has developed, constructed, and now operates, a number of radar facilities at high latitudes. At present, these comprise a system of stations at Tromsø (Norway), Kiruna (Sweden), Sodankylä (Finland), and Longyearbyen (Svalbard). A new system, EISCAT_3D, is currently being constructed.

The Association is fully funded by the Associates, but additional operations may also be funded by short term additional contributions from both Associate and non-Associate bodies. Depending on the available funding, scientific priorities and operational targets are adjusted on an annual basis.

The EISCAT Council is charged with the overall administration and supervision of the Association's activities. The Council appoints a Director, who is responsible for the daily management and operation of the facilities of the Association.

**Operation and scientific development**
The EISCAT Radars delivered a full programme of operations for the user community and operated reliably throughout the year.

The various EISCAT radars operated for a total of 2 043 accounted hours (2 202 hours in 2018).

Common Programmes amounted to 52% (48%) of the operations. Special Programmes amounted to 44% (45%) and other operations amounted to 4% (7%) of the total hours.

IRAP-CNRS (France), KASI (South Korea), KOPRI (South Korea) and IRA-NASU (Ukraine) have Affiliate agreements and totally 12 hours (57 hours) were accounted to the affiliates. The Peer-Review Programme made it possible for user groups from Germany, Russia and USA to run experiments, at no cost, on the systems. Peer-Review time amounted to 58 accounted hours (99 hours).

**Future operation and scientific development**

All systems are ready for users. These include the EISCAT Svalbard Radar, Heating and the UHF and VHF radars with the possibility to run the VHF in tristatic mode by using the antennas in Kiruna and Sodankylä for reception.

The new EISCAT_3D radar system is being constructed. EISCAT_3D will replace the current UHF and VHF radar systems. The new system comprises three phased arrays working together. These will be built in Finland, Norway and Sweden.

The new EISCAT_3D system will be ready for users in 2022. The old UHF and VHF radar systems will be decommissioned at that time.

**Project activities**

A new European Commission funded project, ENVRI-FAIR “Environmental Research Infrastructures building Fair services Accessible for society, Innovation and Research” started 2019-01-01. EISCATs involvement is over four years and totals about 6 MSEK in project funds.

Three European Commission projects, AARC2, COOP_Plus and ENVRI_Plus, ended in 2019.

EISCAT led a consortium comprised of five partners, including EISCAT, which submitted a proposal in response to a H2020 INFRADEV call with deadline in March 2019. The proposal, EISCAT3D-GO was targeted towards “securing the position of EISCAT_3D as an integral part in the scientific community and to realise the full potential of its capabilities to facilitate the needs of the users, both present and potential, when it starts its operations”. The proposal was unfortunately not funded.

**EISCAT_3D project**

The now ongoing EISCAT_3D Stage 1 (E3DS1) construction project is progressing well. Most industry contracts are now in place and ground works at two of the sites, in Skibotn, Norway and Karesuvanto, Finland, were mostly completed by the summer of 2019. The ground works in Skibotn proved to be difficult due to discoveries of quick clay and the resulting cost greatly exceeded the initial estimate. The cost overrun can be absorbed in the overall project planning.

A “programmers team” has now been formed and comprised of 3.5 persons as direct employees plus additional support from Japan. The full E3DS1 project team, including the programmers, amount to 10.5 persons. These positions are funded by the construction project. Regular EISCAT staff and additional support complements the project with an additional 3-4 persons.

The first delivery of the antenna system, for Skibotn, will unfortunately be delayed by one year, meaning installation in 2021 instead of 2020 as planned. This delay may also have consequences for installation at the other two sites, in Finland and Sweden. If so, installation at these sites would then happen in 2022 instead of 2021. The antenna delivery is delayed due to initially some design issues and later to the Corona virus outbreak in P. R. of China, where the units will be manufactured.

The delay will have some financial implications in the project mainly due to the need to keep project staff longer than planned. For the industry deliveries, the delay will mainly be related to a need to possibly store the delivered units near the construction sites for possibly a long period before these can be installed.

An unexpected problem has occurred related to the Swedish site where the local Same village have changed their mind about the location they proposed in 2015. Now they consider the location bad for them. Hopefully, this can be resolved in 2020. If not, an alternative location needs to be found. The primary objective would then be to find a new site in Sweden.

### The work of the Council and its committees

The Council had two ordinary meetings, in June 2019, Tokyo, Japan and in November 2019 Oslo, Norway. The meetings were chaired by Prof. Ingrid Mann.

The regular Council committees, the Administrative and Finance Committee (AFC) and the Scientific Advisory Committee (SAC) both had two meetings each during the year.

### Budget development during the year

The 2019 operations ended a bit below the budgeted target. This was due to fewer scheduled user operations. The radar systems have functioned well and the need for repairs have been even lower than usual. Staff availability has also been high. Two planned staff reductions were implemented as planned. With the construction of EISCAT_3D, the staff needs will change, and a new staff complement plan is being developed for implementation in 2021-2022.

In summary, operating costs were below budget and income was much as expected. In total, the year ended in a net profit.

### The long-term budget plan

The long-term budget plan remains challenging but feasible. The operating cost implications for the *new EISCAT*, with EISCAT_3D as the main system on the mainland, are well understood and with the doubling of the annual contribution from at least the Nordic countries, balanced budgets are within reach, though with less operations than optimal. Additional income via grants or other revenues will be needed to better utilise the new investments.

### The result for 2019 and profit/loss handling

The year ended in a net profit of 2 564 kSEK, which will be added to the designated surplus fund for use in subsequent years.

## PROFIT AND LOSS ACCOUNTS

in thousands of Swedish Crowns

| | Note 1 | *2019* | *2018* |
|---|---|---|---|
| **Income from operations** | | | |
| Grants received | Note 2 | 122 166 | 119 127 |
| Revenue from operations | Note 3 | 0 | 96 |
| Other income from operations | Note 4 | 173 | 762 |
| | | 122 340 | 119 984 |
| **Expenses from operations** | | | |
| Operation costs | Note 5 | -6 748 | -6 481 |
| Administration costs | | -4 207 | -4 102 |
| Personnel costs | Note 6 | -26 390 | -24 066 |
| Depreciation of fixed assets | | -8 938 | -5 116 |
| | | -46 283 | -39 765 |
| **Operating profit/loss** | | **76 056** | **80 220** |
| **Financial items** | | | |
| Interest income | | 675 | 28 |
| Other financial income and cost | | 6 284 | -1 479 |
| | | 6 960 | -1 451 |
| **Net profit/loss for the year** | | **83 016** | **78 769** |
| **Changes in designated funds** | Note 7 | | |
| Net profit/loss for the year | | 83 016 | 78 769 |
| Use of designated investment funds | | -69 177 | -72 047 |
| Use of other designated funds | | 435 | 199 |
| Allocation of unused designated investment and other funds | | -11 710 | -4 989 |
| **Net profit/loss for the year after redistributions** | | **2 564** | **1 933** |

## BALANCE SHEET

in thousands of Swedish Crowns

| | | *2019* | *2018* |
|---|---|---|---|
| **ASSETS** | | | |
| *Fixed assets* | | | |
| **Tangible fixed assets** | Note 8 | | |
| Buildings | | 53 263 | 5 059 |
| Radar systems | | 108 287 | 87 311 |
| Equipment and tools | | 2 258 | 2 261 |
| | | 163 808 | 94 631 |
| **Current assets** | | | |
| Receivables | | 8 585 | 84 555 |
| Prepayments and accrued income | Note 9 | 2 201 | 3 691 |
| Cash at bank and in hand | Note 10 | 246 678 | 131 223 |
| | | 257 463 | 219 470 |
| **Total assets** | | **421 271** | **314 101** |
| **CAPITAL AND LIABILITIES** | | | |
| **Capital** | | | |
| Funds invested | Note 11 | 163 808 | 94 631 |
| Designated funds | Note 12 | 38 135 | 29 395 |
| Net income for the year after redistribution | | 2 564 | 1 933 |
| | | 204 506 | 125 959 |
| **Current liabilities** | | | |
| Accounts payable, trade | | 6 998 | 8 818 |
| EISCAT_3D build grants received but not used | Note 13 | 202 873 | 174 823 |
| External project grants received but not used | Note 14 | 6 465 | 3 907 |
| Other liabilities | | 430 | 595 |
| | | 216 765 | 188 142 |
| **Total capital and liabilities** | | **421 271** | **314 101** |

## STATEMENT OF CASH FLOWS

in thousands of Swedish Crowns

| | *2019* | *2018* |
|---|---:|---:|
| **Operating activities** | | |
| Operating result before financial items | 76 056 | 80 220 |
| Transfer from funds invested | 8 938 | 5 116 |
| | | |
| Interest received | 675 | 28 |
| Currency exchange rate changes | 4 645 | -1 479 |
| Extra ordinary income and cost | 1 640 | 0 |
| | | |
| Increase/decrease of receivables | 75 970 | -60 037 |
| Increase/decrease of prepayments and accrued income | 1 490 | -1 434 |
| Increase/decrease of creditors and liabilities | 28 623 | 109 862 |
| Adjustment for items not included in cash flow | -4 469 | 0 |
| | | |
| **Cash flow from operations** | **193 569** | **132 277** |
| | | |
| **Investment activities** | | |
| Investments in tangible assets | -78 115 | -77 163 |
| | | |
| **Cash flow from investment activities** | **-78 115** | **-77 163** |
| | | |
| **Cash flow for the year** | **115 454** | **55 114** |
| | | |
| **Liquid assets at the beginning of the year** | **131 223** | **76 109** |
| | | |
| **Liquid assets at the end of the year** | **246 678** | **131 223** |

## NOTES *2019* *2018*

**Note 1** *Accounting principles*

The accounting and valuation principles applied are consistent with the provisions of the Swedish Annual Accounts Act and generally accepted accounting principles (for 2017 onwards, bokföringsnämnden allmänna råd och vägledningar, BFNAR 2012:1 K3).

All amounts are in thousands of Swedish kronor (SEK) unless otherwise stated.

*Income*
Received grants are reported as income in the period when they were claimed or received. Conditional grants are recognised as income when the associated conditions have been met. Income and revenue from operations, which include own-account funds, are reported as income when they were claimed or received. Grants and other income in foreign currencies have been accounted in the amounts estimated to be received, based on individual assessment.

*Employee benefits*
Ongoing remuneration to employees, either direct employed or provided via host agreements, in the form of salaries, social security, contributions to pension schemes and staff related insurances are accounted as personnel costs. Other remunerations, in cash, like travel subsistences or as benefits in-kind, like clothing, training and health care are also accounted as personnel costs. Overhead cost on host provided personnel is considered as external services accounted as administration cost.

*Financial income*
Dividends and interest income are accounted when credited the account.

*Receivables*
Receivables are stated at the amounts estimated to be received, based on individual assessment.

*Receivables and payables in foreign currencies*
Receivables and payables in foreign currencies are valued at the closing day rate. Where hedging measures have been used, such as forwarding contracts, the agreed exchange rate is applied. Gains and losses relating to operations are accounted for under other financial income and cost.

*Bank accounts in foreign currencies*
Bank balances in foreign currencies are valued at the closing day rate.

*Fixed assets*
Tangible fixed assets are stated at their original acquisition values after deduction of depreciation according to plan. Assets are depreciated systematically over their estimated useful lives. The following periods of depreciation are applied: Buildings 5 - 50 years, Radar systems 3 - 30 years and Equipment and tools 1 - 5 years.

**Note 2** *Grants received*

The Associates contributed to the operation during the year in accordance with the EISCAT agreement. The Affiliates contributed according to agreed annual commitments. Income from European Commission (EC) funded projects were also accounted as received grants. The E3DS1 project started 2017-09-01 and the resulting projects costs were covered by the funding agencies (see also Note 13). All received project grants are first accounted as prefinancing. Project costs are thereafter covered by withdrawals from prefinancing and at that time accounted as income from operations.

| | *2019* | *2018* |
|---|---:|---:|
| Associates | 23 887 | 23 348 |
| Affiliates | 819 | 811 |
| Project grants, EC | 2 761 | 3 078 |
| Project grant, E3DS1 | 94 699 | 91 890 |
| | 122 166 | 119 127 |

*Accumulated Associate contributions status as of 2019-12-31*

Annual contributions included and for 2019, Finland, Norway and Sweden were credited for providing E3DS1 project related funds. These sums are used for EISCATs ownership and time-share calculation

| | | |
|---|---:|---:|
| Associate P. R. of China | 45 490 | 41 407 |
| Associate Finland | 113 946 | 89 419 |
| Associate Japan | 97 610 | 95 772 |
| Associate Norway | 222 635 | 183 670 |
| Associate Sweden | 238 538 | 191 915 |
| Associate UK | 312 715 | 310 164 |
| Previous Associates | 382 168 | 382 168 |
| | 1 413 102 | 1 294 516 |

**Note 3** *Revenue from operations*

The Association can, at rates related to the costs involved and as available, sell observation hours to Associates, Affiliates and other parties. Income from such selling of time are considered to be revenue. In 2019, no time-buyers used the systems.

| | | |
|---|---:|---:|
| Income from time-buyers | 0 | 96 |

**Note 4** *Other income from operations*

The Association supports visiting users by offering site accommodation and equipment hosting for either campaign brought instruments or for longer deployments. Educational support is done by providing teachers and/or other resources (like laboratory support). Associates and/or user-groups contribute occasionally to system improvements by funding, of own interest, certain repairs or hardware changes.

| | | |
|---|---:|---:|
| Accommodation | 104 | 124 |
| Instrument hosting agreements | 21 | 21 |
| Educational support | 35 | 19 |
| Other income | 13 | 597 |
| | 173 | 762 |

**Note 5** *Operations*

The annual operating target for all systems together is about 2 500 active (high power mode) hours. For 2019, the budget assumed 2 468 hours and the outcome became 1 955 hours. Passive hours come in addition. Such hours have a minimal effect on cost since the systems do not draw more electricity than in an off mode. Accounted hours are usually lower than the sum of operating hours since some systems have a charge rate that is less than 1-to-1.

| *Active hours (high-power), per system* | *Hours* | *Hours* |
|---|---:|---:|
| EISCAT Svalbard Radar | 731 | 897 |
| UHF system | 750 | 880 |
| VHF system | 378 | 199 |
| Heating system | 96 | 97 |
| | 1 955 | 2 072 |
| *Passive hours (receive only)* | | |
| Kiruna receiver system | 202 | 151 |
| Sodankylä receiver system | 202 | 151 |
| | 403 | 302 |

| | 2019 | 2018 |
|---|---|---|
| *Accounted hours* | *Hours* | *Hours* |
| Common programmes | 1 070 | 1 049 |
| Special programmes | 894 | 986 |
| Other hours | 79 | 167 |
| | 2 043 | 2 202 |
| | | |
| *Distribution of special programme hours between Associates* | | |
| Associate P. R. of China | 85 | 110 |
| Associate Finland | 89 | 156 |
| Associate Japan | 146 | 174 |
| Associate Norway | 168 | 216 |
| Associate Sweden | 221 | 147 |
| Associate UK | 187 | 184 |
| | 894 | 986 |
| | | |
| *Distribution, other hours* | | |
| Affiliates | 12 | 57 |
| EISCAT staff and tests | 8 | 4 |
| Per-reviewed campaigns | 59 | 99 |
| Time-buyers | 0 | 8 |
| | 79 | 167 |

**Note 6** *Personnel costs and average number of employees*

The Association employs directly Headquarters and most project staff, currently about 15 positions, including the Director. Of these, six are on shorter-term project employments. The Headquarters is located in Kiruna, Sweden. The personnel working at the Kiruna (Sweden), Sodankylä (Finland), Svalbard and Tromsø (Norway) sites are normally not employed by the Association. Instead, the personnel are provided via site contracts by the Swedish Institute of Space Physics (Kiruna site staff), Oulu University (Sodankylä staff) and the Arctic University of Norway (Tromsø and Svalbard staff). The Association refunds all expenses related to the provided staff, as well as an additional overhead.

| | 2019 | 2018 |
|---|---|---|
| *Personnel costs in total* | | |
| Salaries and emoluments paid to the Director | 2 037 | 1 978 |
| | | |
| Other personnel, employed and provided via site contracts | 16 272 | 14 598 |
| | | |
| Social security contributions amounted to | 7 469 | 6 917 |
| *of which for pension costs* | *3 451* | *3 248* |
| | | |
| Other personnel costs | 612 | 573 |

The Director, Dr. Craig Heinselman, started his employment 2013-01-01. His current employment contract ends 2021-12-31.

Of the pension costs, 354 kSEK (312 kSEK) relates to the Director. He and all other directly employed staff are included in ITP like occupational pension plans. For the personnel provided via site contracts, the pension plans are handled by their respective employer.

The members of the board (EISCAT Council) and members of committees, who represents Associates and Affiliates, do not receive remunerations from the Association. Travel expenses in connection with Council and committee meetings are normally covered by the Associates and Affiliates. The Association reimburses though the travel costs for Committee Chairpersons and external members.

| | 2019 | 2018 |
|---|---|---|
| *Salaries and emoluments and average number of staff per country* | | |
| | | |
| Finland | | |
| Salaries and emoluments | 706 | 678 |
| Average number of staff - men and women | 1 + 0 | 1 + 0 |
| | | |
| Norway (including Svalbard) | | |
| Salaries and emoluments | 5 685 | 5 309 |
| Average number of staff - men and women | 8 + 0 | 9 + 0 |
| | | |
| Sweden | | |
| Salaries and emoluments | 11 919 | 10 589 |
| Average number of staff - men and women | 15 + 2 | 12 + 2 |

*Members of the board and Directors at year-end - men and women*

The board consist of delegations from every Associate country each having a Delegate (formal member) and up to two Representatives.

| | 2019 | 2018 |
|---|---|---|
| Board members (EISCAT Council) | 10 + 4 | 9 + 3 |
| Directors | 1 + 0 | 1 + 0 |

**Note 7** *Changes in designated funds*

Positive numbers - use of designated funds. Negative - transfer to the designated reserves or funds for later use.

| | 2019 | 2018 |
|---|---|---|
| Net profit/loss for the year | 83 016 | 78 769 |
| EISCAT_3D financial gains/losses taken in project finances | -4 469 | 0 |
| Changes to capital operating reserve | -1 375 | 182 |
| Changes to decommissioning fund | -2 479 | -2 446 |
| Changes to E3D construction reserve | -3 176 | -3 134 |
| Changes to funds invested | -69 177 | -72 047 |
| Changes to spare parts reserve | 4 | 18 |
| Changes to surplus fund | 219 | 590 |
| | 2 564 | 1 933 |

**Note 8** *Tangible fixed assets*

Changes in tangible fixed assets.

| | 2019 | 2018 |
|---|---|---|
| Buildings | | |
| Opening acquisition value | 46 021 | 42 478 |
| Acquisitions during the year | 48 707 | 3 544 |
| Disposals during the year | -152 | 0 |
| Closing acquisition value | 94 576 | 46 021 |
| | | |
| Opening accumulated depreciation | -40 963 | -40 670 |
| Depreciations during the year | -502 | -293 |
| Disposals during the year | 152 | 0 |
| Closing accumulated depreciation | -41 313 | -40 963 |
| | | |
| Closing residual value | 53 263 | 5 059 |
| | | |
| Radar systems | | |
| Opening acquisition value | 337 357 | 250 760 |
| Acquisitions during the year | 28 348 | 86 597 |
| Disposals during the year | 0 | 0 |
| Closing acquisition value | 365 705 | 337 357 |
| | | |
| Opening accumulated depreciation | -250 047 | -246 480 |
| Depreciations during the year | -7 371 | -3 566 |
| Disposals during the year | 0 | 0 |
| Closing accumulated depreciation | -257 417 | -250 047 |
| | | |
| Closing residual value | 108 287 | 87 311 |

| | 2019 | 2018 |
|---|---|---|
| Equipment and tools | | |
| Opening acquisition value | 35 652 | 34 992 |
| Acquisitions during the year | 1 061 | 687 |
| Disposals during the year | -368 | -27 |
| Closing acquisition value | 36 345 | 35 652 |
| | | |
| Opening accumulated depreciation | -33 391 | -32 161 |
| Depreciations during the year | -1 065 | -1 257 |
| Disposals during the year | 368 | 27 |
| Closing accumulated depreciation | -34 087 | -33 391 |
| | | |
| Closing residual value | 2 258 | 2 261 |
| | | |
| Sum tangible fixed assets | 163 808 | 94 631 |

**Note 9** *Prepayments and accrued income*

Resources in staff and direct costs spent in ongoing externally funded projects are covered by accrued income until settled by submission of periodic report claims. In 2019 the ENRVI-FAIR project started and AARC2, COOP_Plus and ENVRI_Plus projects ended.

| | 2019 | 2018 |
|---|---|---|
| Prepaid rents | 9 | 1 |
| Prepaid insurances | 798 | 698 |
| Accrued income, previous projects | 0 | 2 164 |
| Accrued income, ENVRI-FAIR project | 780 | 0 |
| Accrued income, EOSC-hub project | 544 | 710 |
| Other items | 69 | 118 |
| | 2 201 | 3 691 |

**Note 10** *Bank balances status*

| | 2019 | 2018 |
|---|---|---|
| Nordea | 246 678 | 131 223 |
| Cash in hand | 0 | 0 |
| | 246 678 | 131 223 |

**Note 11** *Funds invested status*

| | 2019 | 2018 |
|---|---|---|
| Buildings | 53 263 | 5 059 |
| Radar Systems | 108 287 | 87 311 |
| Equipment and Tools | 2 258 | 2 261 |
| | 163 808 | 94 631 |

**Note 12** *Designated funds*

The designated funds are divided into eight funds and reserves. The capital operating and spare parts reserves are used to manage required purchases between years, including unbudgeted ones. The surplus fund is used to manage overall profits and losses between years. The other funds are earmarked for specific purposes.

| | 2019 | 2018 |
|---|---|---|
| Capital operating reserve | 3 131 | 1 755 |
| E3D construction reserve | 6 309 | 3 134 |
| Decommissioning fund | 4 924 | 2 446 |
| Equipment repair fund | 754 | 754 |
| Investment fund | 7 753 | 7 753 |
| Restructuring reserve | 4 101 | 4 101 |
| Spare parts reserve | 97 | 101 |
| Surplus fund | 11 065 | 9 351 |
| | 38 135 | 29 395 |

**Note 13** *EISCAT_3D build grants received but not used*

The construction project, E3DS1, started 2017-09-01 and its first phase, Stage 1, will be completed in 2022. Most Associates have now committed to its realisation. Two E3DS1 specific funding payments were received in 2019. The funds are kept as prefinancing until used in the project. Funds spent are deducted from the different funding sources in accordance with the agreed funding plan.

Changes in EISCAT_3D build grants received but not used

| | 2019 | 2018 |
|---|---|---|
| Associate Finland | | |
| Opening balance | 41 109 | 0 |
| Received during the year | 0 | 41 109 |
| Used during the year | -20 555 | 0 |
| Closing balance | 20 555 | 41 109 |
| | | |
| Associate Norway | | |
| Opening balance | 66 381 | 0 |
| Received during the year | 88 280 | 66 381 |
| Used during the year | -33 191 | 0 |
| Closing balance | 121 470 | 66 381 |
| | | |
| Associate Sweden | | |
| Opening balance | 67 332 | 39 980 |
| Received during the year | 30 000 | 50 000 |
| Used during the year | -40 953 | -22 648 |
| Closing balance | 56 379 | 67 332 |
| | | |
| Associate UK | | |
| Opening balance | 0 | 15 455 |
| Received during the year | 0 | 53 787 |
| Used during the year | 0 | -69 242 |
| Closing balance | 0 | 0 |
| | | |
| E3DS1 project finances, gains/losses | 4 469 | 0 |
| | | |
| Sum EISCAT_3D received build grants | 202 873 | 174 823 |

**Note 14** *External project grants received but not used*

All externally funded projects work with prefinancing. For European Commission projects, these are in EUR's. The prefinancing is used to cover reported and approved costs. AARC2 and COOP_Plus were financially concluded during 2019. Prefinancing for ENVRI-FAIR was received.

| | 2019 | 2018 |
|---|---|---|
| Previous projects, prefinancing | 0 | 1 167 |
| ENVRI-FAIR H2020 prefinancing | 2 777 | 0 |
| ENVRI_Plus H2020 prefinancing | 1 539 | 1 509 |
| EOSC-hub prefinancing | 2 149 | 1 230 |
| | 6 465 | 3 907 |

# Appendix:

# EISCAT Scientific Association Annual Report, 2020

EISCAT Scientific Association
Registered as a Swedish non-profit organisation
Organisation number: 897300-2549

Annual financial report for the year 2020-01-01 – 2020-12-31

The EISCAT Council and the Director for the Association submits herewith the annual report for 2020.

# ADMINISTRATION REPORT

**Ownership, organisation and objective**

The EISCAT Scientific Association was established in 1975 through an agreement between six European organisations. Japan joined in 1996 and the People's Republic of China in 2007.

The EISCAT Associates at 2020-12-31 are: China Research Institute of Radiowave Propagation (People's Republic of China), National Institute of Polar Research (Japan), Norges forskningsråd (Norway), Suomen Akatemia (Finland), UK Research and Innovation (United Kingdom of Great Britain and Northern Ireland) and Vetenskapsrådet (Sweden).

The now-running EISCAT Agreement came into force 2017-06-20, with all Associates making long term funding commitments to the Association. The Association has its formal seat in Kiruna, Sweden, and is registered as a non-profit organisation.

The aim of the Association is to make significant progress in the understanding of physical processes in geospace, in the high latitude atmosphere, and in the coupling between the high and low latitudes and altitudes. For this purpose, the Association has developed, constructed, and now operates, a number of radar facilities at high latitudes. At present, these comprise a system of stations at Tromsø (Norway), Kiruna (Sweden), Sodankylä (Finland), and Longyearbyen (Svalbard). The new system, EISCAT_3D, is currently being constructed.

The Association is fully funded by the Associates, but additional operations may also be funded by short term additional contributions from both Associate and non-Associate bodies. Depending on the available funding, scientific priorities and operational targets are adjusted on an annual basis.

The EISCAT Council is charged with the overall administration and supervision of the Association's activities. The Council appoints a Director, who is responsible for the daily management and operation of the facilities of the Association.

**Operation and scientific development**

The EISCAT Radars systems operated reliably throughout the year and 1 918 hours were accounted in 2020 (2 043 hours in 2019).

Common Programmes amounted to 49% (52%) of the operations. Special Programmes amounted to 44% (44%) and other operations amounted to 7% (4%) of the total hours.

CNRS-IRAP (France), DLR-SO (Germany), IRA-NASU (Ukraine), JHUAPL (USA), KASI (South Korea) and KOPRI (South Korea) have Affiliate agreements and totally 52 hours (12 hours) were accounted to the affiliates. Both DLR-SO and JHUAPL joined the Association as Affiliates during 2020. The Peer-Review Programme made it possible for user groups from P. R of China, France, Germany, Norway and Russia to run experiments, at no cost, on the systems. Peer-Review time amounted to 72 accounted hours (58 hours).

**Future operation and scientific development**

The current EISCAT systems are ready for users. These include the EISCAT Svalbard Radar, Heating and the UHF and VHF radars with the possibility to run the VHF in tristatic mode by using the antennas in Kiruna and Sodankylä for reception.

The new EISCAT_3D radar system is being constructed. EISCAT_3D will replace the current UHF and VHF radar systems. The new system comprises three phased arrays working together. These will be built in Finland, Norway and Sweden. The new EISCAT_3D system will be ready for users by the end of 2022. The old UHF and VHF radar systems will be decommissioned at that time.

**Project activities**

The two ongoing European Commission funded projects, ENVRI-FAIR and EOSC-Hub continued throughout the year.

Two new European Commission funded projects will start in 2021, EGI-ACE and PITHIA-NRF. EGI-ACE, “EGI Advanced Computing for EOSC”, is under *the Implementing the European Open Science Cloud* call and will start in January 2021 and will run for 30 months. EISCATs involvement is for five person months and about 650 kSEK in project funds. PITHIA-NRF, “Plasmasphere Ionosphere Thermosphere Integrated Research Environment and Access services: a Network of Research Facilities” is under the *Integrating and opening research infrastructures of European interest* call. The project will start in April 2021 and will run for four years. EISCATs involvement is for about four staff-years and 6 MSEK in project funds. EISCAT will be involved in various tasks in the PITHIA-NRF project, including leading the Transnational Access part.

**EISCAT_3D project**

The ongoing EISCAT_3D Stage 1 (E3DS1) construction project is progressing well, and all major industry contracts are now in place and mass-production of most sub-systems have started. The parts needed for installation in Skibotn in autumn 2021 will have all been manufactured well before the need date. Production of the units for Finland and Sweden have also started. Since the installation is delayed, some of these units will need to be stored in factory before shipped to the designated locations.

The problem related to the Swedish site was resolved towards the end of the year and, providing that the tender for ground works will prove successful, the third EISCAT_3D site will be prepared during 2021 such that it is ready for system installation in 2022.

The overall schedule remains untouched meaning that the Chinese manufacturer of the antenna system will install it in Norway in 2021 followed by installations in Finland and Sweden in 2022. The radar electronics, which are produced in Finland and Sweden, will be installed in the antenna systems directly after. Since the COVID-19 pandemic is still ongoing, a crucial milestone will be the shipment, and subsequent arrival of the units and the Chinese crew, to Norway for installation of the antenna system during summer 2021. If this fails due to border restrictions, then there will be a further delay in the project. Since the installation of the antenna system require reasonable weather conditions, it could mean a full season delay.

The third tendering round for the buildings resulted finally in multiple bids and a vendor could be chosen. It will be the same contractor, from Finland, providing turnkey buildings at all three EISCAT_3D locations, starting with constructions in Norway summer 2021.

**The work of the Council and its committees**

Due to COVID-19 all Council and Committee meetings were held digitally. Council met in spring and autumn and the meetings were chaired by Prof. Ingrid Mann. In addition to regular matters, Council decided to start the process of hiring a new Director to join in 2023. Council decided also to extend the employment of the current Director, Dr. Craig Heinselman for one more year. Dr. Heinselman's employment will now end 2022-12-31. At the end of the year, Prof. Mann handed over the chairpersonship to Prof. Anita Aikio from Finland. Prof. Aikio will be the Council Chairperson for two years, 2021 - 2022.

The regular Council committees, the Administrative and Finance Committee (AFC) and the Scientific Advisory Committee (SAC) both had two digital meetings each during the year.

**Budget development during the year**

The 2020 operations ended below the budgeted target. This was much due to users travel restrictions. Likewise, the same restrictions meant almost no travels by EISCAT staff resulting in a substantial cost reduction. A substantial water leak in the building on Svalbard resulted in major repairs. The leak was accepted as damage by the insurance company and a partial coverage of the repair cost is expected in 2021.

Since staff needs on Svalbard are now only two persons, one of the staff quarters were sold leaving two remaining. The selling of the accommodation added income.

Two new Affiliates joined the Association. The Institute for Solar-Terrestrial Physics of the German Aerospace Center (DLR-SO), Germany, joined in January and the Johns Hopkins University Applied Physics Laboratory LLC (JHUAPL), USA, joined in April. Both paid operating contributions in 2020 and DLR-SO made also a payment towards EISCAT_3D.

The Japanese Associate, National Institute of Polar Research, could finally commit to EISCAT_3D funding and three instalments from Japan were received.

In summary, less operating costs and more income meant that the year ended in a net profit.

**The long-term budget plan**

The long-term budget plan remains on a challenging but feasible level. The operating cost implications for the *new EISCAT*, with EISCAT_3D as the main system on the mainland, are well understood and with the doubling of the annual contribution from at least the Nordic countries, mean that the first years in the five-year plan can be balanced, though with less operations than optimal. Additional income via grants or other revenues will be needed to better utilise the new investments.

**The result for 2020 and profit/loss handling**

The year ended in a net profit of 3 118 kSEK, which will be added to the designated surplus fund for use in subsequent years.

## PROFIT AND LOSS ACCOUNTS

in thousands of Swedish Crowns

| | Note 1 | *2020* | *2019* |
|---|---|---|---|
| **Income from operations** | | | |
| Grants received | Note 2 | 93 961 | 122 166 |
| Revenue from operations | Note 3 | 0 | 0 |
| Other income from operations | Note 4 | 81 | 173 |
| | | 94 042 | 122 340 |
| **Expenses from operations** | | | |
| Operation costs | Note 5 | -7 797 | -6 748 |
| Administration costs | | -2 711 | -4 207 |
| Personnel costs | Note 6 | -26 021 | -26 390 |
| Depreciation of fixed assets | | -8 799 | -8 938 |
| | | -45 328 | -46 283 |
| **Operating profit/loss** | | **48 714** | **76 056** |
| **Financial items** | | | |
| Interest income | | 203 | 675 |
| Other financial income and cost | | -7 520 | 4 645 |
| | | -7 317 | 5 320 |
| **Other items** | | | |
| Income from sold inventory | | 2 462 | 1 640 |
| **Net profit/loss for the year** | | **43 859** | **83 016** |

| | | | |
|---|---|---|---|
| **Changes in designated funds** | Note 7 | | |
| Net profit/loss for the year | | 43 859 | 83 016 |
| Use of designated investment funds | | -43 087 | -69 177 |
| Use of other designated funds | | -216 | 435 |
| Allocation of unused designated investment and other funds | | 2 562 | -11 710 |
| **Net profit/loss for the year after redistributions** | | **3 118** | **2 564** |

## BALANCE SHEET

in thousands of Swedish Crowns

| | | 2020 | 2019 |
|---|---|---|---|
| **ASSETS** | | | |
| *Fixed assets* | | | |
| **Tangible fixed assets** | Note 8 | | |
| Buildings | | 55 223 | 53 263 |
| Radar systems | | 149 536 | 108 287 |
| Equipment and tools | | 2 115 | 2 258 |
| | | 206 874 | 163 808 |
| **Current assets** | | | |
| Receivables | | 37 479 | 8 585 |
| Prepayments and accrued income | Note 9 | 3 179 | 2 201 |
| Cash at bank and in hand | Note 10 | 313 546 | 246 678 |
| | | 354 203 | 257 463 |
| **Total assets** | | **561 078** | **421 271** |
| **CAPITAL AND LIABILITIES** | | | |
| **Capital** | | | |
| Funds invested | Note 11 | 206 874 | 163 808 |
| Designated funds | Note 12 | 44 682 | 38 135 |
| Net income for the year after redistribution | | 3 118 | 2 564 |
| | | 254 674 | 204 506 |
| **Current liabilities** | | | |
| Accounts payable, trade | | 22 362 | 6 998 |
| EISCAT_3D build grants received but not used | Note 13 | 279 303 | 202 873 |
| External project grants received but not used | Note 14 | 3 777 | 6 465 |
| Other liabilities | | 961 | 430 |
| | | 306 404 | 216 765 |
| **Total capital and liabilities** | | **561 078** | **421 271** |

## STATEMENT OF CASH FLOWS

in thousands of Swedish Crowns

| | *2020* | *2019* |
|---|---:|---:|
| **Operating activities** | | |
| Operating result before financial items | 48 714 | 76 056 |
| Transfer from funds invested | 8 799 | 8 938 |
| | | |
| Interest received | 203 | 675 |
| Financial income and cost | -7 520 | 4 645 |
| Other income and cost | 2 462 | 1 640 |
| | | |
| Increase/decrease of receivables | -28 894 | 75 970 |
| Increase/decrease of prepayments and accrued income | -978 | 1 490 |
| Increase/decrease of creditors and liabilities | 89 638 | 28 623 |
| Adjustment for items not included in cash flow | 6 329 | -4 469 |
| | | |
| **Cash flow from operations** | **118 754** | **193 569** |
| | | |
| **Investment activities** | | |
| Investments in tangible assets | -51 886 | -78 115 |
| | | |
| **Cash flow from investment activities** | **-51 886** | **-78 115** |
| | | |
| **Cash flow for the year** | **66 868** | **115 454** |
| | | |
| **Liquid assets at the beginning of the year** | **246 678** | **131 223** |
| | | |
| **Liquid assets at the end of the year** | **313 546** | **246 678** |

**NOTES** *2020* *2019*

**Note 1** *Accounting principles*

The accounting and valuation principles applied are consistent with the provisions of the Swedish Annual Accounts Act and generally accepted accounting principles (for 2017 onwards, bokföringsnämnden allmänna råd och vägledningar, BFNAR 2012:1 K3).

All amounts are in thousands of Swedish kronor (SEK) unless otherwise stated.

*Income*
Received grants are reported as income in the period when they were claimed or received. Conditional grants are recognised as income when the associated conditions have been met. Income and revenue from operations, which include own-account funds, are reported as income when they were claimed or received. Grants and other income in foreign currencies have been accounted in the amounts estimated to be received, based on individual assessment.

*Employee benefits*
Ongoing remuneration to employees, either direct employed or provided via host agreements, in the form of salaries, social security, contributions to pension schemes and staff related insurances are accounted as personnel costs. Other remunerations, in cash, like travel subsistences or as benefits in-kind, like clothing, training and health care are also accounted as personnel costs. Overhead cost on host provided personnel is considered as external services accounted as administration cost.

*Financial income*
Dividends and interest income are accounted when credited the account.

*Receivables*
Receivables are stated at the amounts estimated to be received, based on individual assessment.

*Receivables and payables in foreign currencies*
Receivables and payables in foreign currencies are valued at the closing day rate. Where hedging measures have been used, such as forwarding contracts, the agreed exchange rate is applied. Gains and losses relating to operations are accounted for under other financial income and cost.

*Bank accounts in foreign currencies*
Bank balances in foreign currencies are valued at the closing day rate.

*Fixed assets*
Tangible fixed assets are stated at their original acquisition values after deduction of depreciation according to plan. Assets are depreciated systematically over their estimated useful lives. The following periods of depreciation are applied: Buildings 5 - 50 years, Radar systems 3 - 30 years and Equipment and tools 1 - 5 years.

**Note 2** *Grants received*

The Associates contributed to the operation during the year in accordance with the EISCAT agreement. The Affiliates contributed according to agreed annual commitments. Income from European Commission (EC) funded projects were also accounted as received grants. The E3DS1 project started 2017-09-01 and the resulting projects costs were covered by the Associates (see Note 13) and other funds. Received project grants from the Associates are first accounted as prefinancing. Project costs are thereafter covered by withdrawals from prefinancing and at that time accounted as income from operations.

| | *2020* | *2019* |
|---|---|---|
| Associates | 24 328 | 23 887 |
| Affiliates | 904 | 819 |
| Project grants, EC | 2 401 | 2 761 |
| Project grant, E3DS1 | 66 328 | 94 699 |
| | 93 961 | 122 166 |

*Accumulated Associate contributions status as of 2020-12-31*
Annual contributions included and for 2020, Finland, Japan (as in-kind), Norway and Sweden were credited for providing E3DS1 project-related funds. These sums are used for EISCATs ownership and time-share calculation

| | *2020* | *2019* |
|---|---|---|
| Associate P. R. of China | 49 434 | 45 490 |
| Associate Finland | 132 376 | 113 946 |
| Associate Japan | 100 595 | 97 610 |
| Associate Norway | 251 539 | 222 635 |
| Associate Sweden | 262 717 | 238 538 |
| Associate UK | 315 284 | 312 715 |
| Previous Associates | 382 168 | 382 168 |
| | 1 494 113 | 1 413 102 |

**Note 3** *Revenue from operations*

The Association can, at rates related to the costs involved and as available, sell observation hours to Associates, Affiliates and other parties. Income from such selling of time are considered to be revenue. In 2020, no time-buyers used the systems.

| | *2020* | *2019* |
|---|---|---|
| Income from time-buyers | 0 | 0 |

**Note 4** *Other income from operations*

The Association supports visiting users by offering site accommodation and equipment hosting for either campaign brought instruments or for longer deployments. Educational support is done by providing teachers and/or other resources (like laboratory support). Associates and/or user-groups contribute occasionally to system improvements by funding, of own interest, certain repairs or hardware changes.

| | *2020* | *2019* |
|---|---|---|
| Accommodation | 44 | 104 |
| Instrument hosting agreements | 21 | 21 |
| Educational support | 16 | 35 |
| Other income | 0 | 13 |
| | 81 | 173 |

**Note 5** *Operations*

The annual operating target for all systems together is about 2 500 active (high power mode) hours. For 2020, the budget assumed 2 468 hours and the outcome became 1 863 hours. Passive hours come in addition. Such hours have a minimal effect on cost since the systems do not draw more electricity than in an off mode. Accounted hours are usually lower than the sum of operating hours since some systems have a charge rate that is less than 1-to-1.

| *Active hours (high-power), per system* | *Hours* | *Hours* |
|---|---|---|
| EISCAT Svalbard Radar | 700 | 731 |
| UHF system | 743 | 750 |
| VHF system | 330 | 378 |
| Heating system | 91 | 96 |
| | 1 863 | 1 955 |
| *Passive hours (receive only)* | | |
| Kiruna receiver system | 134 | 202 |
| Sodankylä receiver system | 134 | 202 |
| | 268 | 403 |

| | 2020 | 2019 |
|---|---|---|
| *Accounted hours* | *Hours* | *Hours* |
| Common programmes | 946 | 1 070 |
| Special programmes | 848 | 894 |
| Other hours | 125 | 79 |
| | 1 918 | 2 043 |
| | | |
| *Distribution of special programme hours between Associates* | | |
| Associate P. R. of China | 0 | 76 |
| Associate Finland | 131 | 82 |
| Associate Japan | 132 | 134 |
| Associate Norway | 111 | 154 |
| Associate Sweden | 180 | 199 |
| Associate UK | 205 | 157 |
| All Associates, AA-runs | 91 | 94 |
| | 848 | 894 |
| | | |
| *Distribution, other hours* | | |
| Affiliates | 52 | 12 |
| EISCAT staff and tests | 0 | 8 |
| Per-reviewed campaigns | 73 | 59 |
| Time-buyers | 0 | 0 |
| | 125 | 79 |

**Note 6** *Personnel costs and average number of employees*

The Association employs directly Headquarters and most project staff, currently about 15 positions, including the Director. Of these, five are on shorter-term project employments. The Headquarters is located in Kiruna, Sweden. The personnel working at the Kiruna (Sweden), Sodankylä (Finland), Svalbard and Tromsø (Norway) sites are normally not employed by the Association. Instead, the personnel are provided via site contracts by the Swedish Institute of Space Physics (Kiruna site staff), Oulu University (Sodankylä staff) and the Arctic University of Norway (Tromsø and Svalbard staff). The Association refunds all expenses related to the provided staff, as well as an additional overhead.

| | 2020 | 2019 |
|---|---|---|
| *Personnel costs in total* | | |
| Salaries and emoluments paid to the Director | 2 087 | 2 037 |
| | | |
| Other personnel, employed and provided via site contracts | 15 915 | 16 272 |
| | | |
| Social security contributions amounted to | 7 843 | 7 469 |
| *of which for pension costs* | *3 943* | *3 451* |
| | | |
| Other personnel costs | 177 | 612 |

The Director, Dr. Craig Heinselman, started his employment 2013-01-01. His current employment contract ends 2021-12-31. It will be extended one year.

Of the pension costs, 380 kSEK (354 kSEK) relates to the Director. He and all other directly employed staff are included in ITP like occupational pension plans. For the personnel provided via site contracts, the pension plans are handled by their respective employer.

The members of the board (EISCAT Council) and members of committees, who represents Associates and Affiliates, do not receive remunerations from the Association. Travel expenses in connection with Council and committee meetings are normally covered by the Associates and Affiliates. The Association reimburses though the travel costs for Committee Chairpersons and external members.

| | 2020 | 2019 |
|---|---|---|
| *Salaries and emoluments and average number of staff per country* | | |
| | | |
| Finland | | |
| Salaries and emoluments | 704 | 706 |
| Average number of staff - men and women | 1 + 0 | 1 + 0 |
| | | |
| Norway (including Svalbard) | | |
| Salaries and emoluments | 4 605 | 5 685 |
| Average number of staff - men and women | 8 + 0 | 8 + 0 |
| | | |
| Sweden | | |
| Salaries and emoluments | 12 693 | 11 919 |
| Average number of staff - men and women | 15 + 2 | 15 + 2 |

*Members of the board and Directors at year-end - men and women*

The board consist of delegations from every Associate country each having a Delegate (formal member) and up to two Representatives.

| | 2020 | 2019 |
|---|---|---|
| Board members (EISCAT Council) | 10 + 4 | 10 + 4 |
| Directors | 1 + 0 | 1 + 0 |

**Note 7** *Changes in designated funds*

Positive numbers - use of designated funds. Negative - transfer to the designated reserves or funds for later use.

| | 2020 | 2019 |
|---|---|---|
| Net profit/loss for the year | 43 859 | 83 016 |
| EISCAT_3D financial gains/losses taken in project finances | 6 329 | -4 469 |
| Changes to capital operating reserve | 74 | -1 375 |
| Changes to decommissioning fund | -1 651 | -2 479 |
| Changes to E3D construction reserve | -2 116 | -3 176 |
| Changes to funds invested | -43 087 | -69 177 |
| Changes to spare parts reserve | 13 | 4 |
| Changes to surplus fund | -303 | 219 |
| | 3 118 | 2 564 |

**Note 8** *Tangible fixed assets*

Changes in tangible fixed assets.

| | 2020 | 2019 |
|---|---|---|
| Buildings | | |
| Opening acquisition value | 94 576 | 46 021 |
| Acquisitions during the year | 2 456 | 48 707 |
| Disposals during the year | -632 | -152 |
| Closing acquisition value | 96 400 | 94 576 |
| | | |
| Opening accumulated depreciation | -41 313 | -40 963 |
| Depreciations during the year | -495 | -502 |
| Disposals during the year | 632 | 152 |
| Closing accumulated depreciation | -41 177 | -41 313 |
| | | |
| Closing residual value | 55 223 | 53 263 |
| | | |
| Radar systems | | |
| Opening acquisition value | 365 705 | 337 357 |
| Acquisitions during the year | 48 455 | 28 348 |
| Disposals during the year | -8 | 0 |
| Closing acquisition value | 414 152 | 365 705 |
| | | |
| Opening accumulated depreciation | -257 417 | -250 047 |
| Depreciations during the year | -7 206 | -7 371 |
| Disposals during the year | 8 | 0 |
| Closing accumulated depreciation | -264 616 | -257 417 |
| | | |
| Closing residual value | 149 536 | 108 287 |

| | 2020 | 2019 |
|---|---|---|
| Equipment and tools | | |
| Opening acquisition value | 36 345 | 35 652 |
| Acquisitions during the year | 975 | 1 061 |
| Disposals during the year | -1 014 | -368 |
| Closing acquisition value | 36 306 | 36 345 |
| | | |
| Opening accumulated depreciation | -34 087 | -33 391 |
| Depreciations during the year | -1 097 | -1 065 |
| Disposals during the year | 993 | 368 |
| Closing accumulated depreciation | -34 191 | -34 087 |
| | | |
| Closing residual value | 2 115 | 2 258 |
| | | |
| Sum tangible fixed assets | 206 874 | 163 808 |

**Note 9** *Prepayments and accrued income*

Resources in staff and direct costs spent in ongoing externally funded projects are covered by accrued income until settled by submission of periodic report claims. In 2020, the ENRVI-FAIR and EOSC-hub projects continued throughout the year.

| | 2020 | 2019 |
|---|---|---|
| Prepaid rents | 9 | 9 |
| Prepaid insurances | 789 | 798 |
| Accrued income, previous projects | 0 | 0 |
| Accrued income, ENVRI-FAIR project | 638 | 780 |
| Accrued income, EOSC-hub project | 1 672 | 544 |
| Other items | 70 | 69 |
| | 3 179 | 2 201 |

**Note 10** *Bank balances status*

| | 2020 | 2019 |
|---|---|---|
| Nordea | 313 546 | 246 678 |
| Cash in hand | 0 | 0 |
| | 313 546 | 246 678 |

**Note 11** *Funds invested status*

| | 2020 | 2019 |
|---|---|---|
| Buildings | 55 223 | 53 263 |
| Radar Systems | 149 536 | 108 287 |
| Equipment and Tools | 2 115 | 2 258 |
| | 206 874 | 163 808 |

**Note 12** *Designated funds*

The designated funds are divided into eight funds and reserves. The capital operating and spare parts reserves are used to manage required purchases between years, including unbudgeted ones. The surplus fund is used to manage overall profits and losses between years. The other funds are earmarked for specific purposes.

| | 2020 | 2019 |
|---|---|---|
| Capital operating reserve | 3 057 | 3 131 |
| E3D construction reserve | 8 425 | 6 309 |
| Decommissioning fund | 6 576 | 4 924 |
| Equipment repair fund | 754 | 754 |
| Investment fund | 7 753 | 7 753 |
| Restructuring reserve | 4 101 | 4 101 |
| Spare parts reserve | 84 | 97 |
| Surplus fund | 13 931 | 11 065 |
| | 44 682 | 38 135 |

**Note 13** *EISCAT_3D build grants received but not used*

The construction project, E3DS1, started 2017-09-01 and its first phase, Stage 1, will be completed in 2022. Most Associates have now committed to its realisation. E3DS1 specific funding payments from Japan, Finland and Norway were received in 2020. Associate funds are kept as prefinancing until used in the project. Funds spent are deducted from the different funding sources in accordance with the agreed funding plan. United Kingdom contributed to the construction project during 2017-2018 and the funds were also used during that period.

Changes in EISCAT_3D build grants received but not used

| | 2020 | 2019 |
|---|---|---|
| Associate Finland | | |
| Opening balance | 20 555 | 41 109 |
| Received during the year | 36 817 | 0 |
| Used during the year | -14 424 | -20 555 |
| Closing balance | 42 948 | 20 555 |
| | | |
| Associate Japan | | |
| Opening balance | 0 | 0 |
| Received during the year | 23 765 | 0 |
| Used during the year | 0 | 0 |
| Closing balance | 23 765 | 0 |
| | | |
| Associate Norway | | |
| Opening balance | 121 470 | 66 381 |
| Received during the year | 78 398 | 88 280 |
| Used during the year | -23 288 | -33 191 |
| Closing balance | 176 580 | 121 470 |
| | | |
| Associate Sweden | | |
| Opening balance | 56 379 | 67 332 |
| Received during the year | 0 | 30 000 |
| Used during the year | -18 509 | -40 953 |
| Closing balance | 37 870 | 56 379 |
| | | |
| E3DS1 project finances, gains/losses | | |
| Opening balance | 4 469 | 0 |
| Changes during the year | -6 329 | 4 469 |
| Closing balance | -1 861 | 4 469 |
| | | |
| Sum EISCAT_3D received build grants | 279 303 | 202 873 |

**Note 14** *External project grants received but not used*

All externally funded projects work with prefinancing. For European Commission projects, these are in EUR's. The prefinancing is used to cover reported and approved costs. ENVRI_Plus were financially concluded during 2020.

| | 2020 | 2019 |
|---|---|---|
| ENVRI-FAIR H2020 prefinancing | 2 667 | 2 777 |
| ENVRI_Plus H2020 prefinancing | 0 | 1 539 |
| EOSC-hub prefinancing | 1 110 | 2 149 |
| | 3 777 | 6 465 |

Report 2019–2020 of the EISCAT Scientific Association

EISCAT Headquarters
Box 812, SE-981 28 Kiruna, Sweden

Scientific contributions: EISCAT Associates and staff

# The EISCAT Associates and Affiliates

December 2020

## CRIRP

China Research Institute of Radiowave Propagation
China
*www.crirp.ac.cn*

## NFR

Forskningsrådet
Norway
*www.forskningsradet.no*

## NIPR

National Institute of Polar Research
Japan
*www.nipr.ac.jp*

## SA

Suomen Akatemia
Finland
*www.aka.fi*

## UKRI

UK Research and Innovation
United Kingdom
*www.ukri.org*

## VR

Vetenskapsrådet
Sweden
*www.vr.se*

## CNRS-IRAP

Institut de Recherche en Astrophysique et Planétologie, France
*www.irap.omp.eu*

## DLR-SO

Institut für Solar-Terrestrische Physik, Germany
*www.dlr.de/so*

## KASI

Korea Astronomy and Space Science Institute, South Korea
*www.kasi.re.kr*

## KOPRI

Korea Polar Research Institute, South Korea
*www.kopri.re.kr*

## JHUAPL

Johns Hopkins University Applied Physics Laboratory, United States
*www.jhuapl.edu*

# EISCAT Scientific Association

## Headquarters

EISCAT Scientific Association
Bengt Hultqvists väg 1
SE-981 92 Kiruna
Sweden
Phone: +46 980 79150
*www.eiscat.se*

## Sites

### Kiruna

EISCAT Kiruna Site
EISCAT Mottagarstation
SE-981 92 Kiruna
Sweden

### Longyearbyen

EISCAT Svalbard Radar
Breinosa, Gruve7-veien
N-9171 Longyearbyen
Norway

### Sodankylä

EISCAT Sodankylä Site
Tähteläntie 54B
FIN-996 00 Sodankylä
Finland

### Tromsø

EISCAT Tromsø Site
Ramfjordmoen
N-9027 Ramfjordbotn
Norway